Mapping and quantification of extension and vertical displacements in the inner Oslofjord

Nicolai Marthinsen

Master Thesis in Geosciences

Structural Geology and Tectonics

60 credits

Department of Geosciences

Faculty of Mathematics and Natural Sciences

UNIVERSITY OF OSLO

June 2018

Supervisors: Lars Eivind Augland & Anders Mattias Lundmark

Title: Mapping and quantification of extension and vertical displacements in the inner Oslofjord

Author: Nicolai Marthinsen

This thesis is published digitally through DUO – Digitale utgivelser ved UiO and BIBSYS at the following addresses:

http://www.duo.uio.no/

Print: Reprosentralen, Universitetet i Oslo

Abstract

The goal of this thesis is to estimate the amount of extension and displacement across a segment of the inner Oslofjord, Norway using field mapping of exstensional structures and geometrical constraints.

The mapped area is dominated by middle Ordovician to lower Silurian sediments folded during the development of the Scandinavian Caledonides, followed by the development of the Oslo Rift in the late Carboniferous. Rifting led to the formation of extensional structures and magmatic intrusions. The recorded fault planes and dikes throughout the study area typically show a NNW-SSE trending orientation. Extension in the study area has been calculated using different trigonometrical methods, which suggest 10-15% stretching across the field area. These results correlates well with some previous estimates across the entire Oslo Graben.

Based on observations in field and data processing, different hypothesis have been tested to interpret how the Oslo Rift developed.

Preface

This master thesis is the final work after one year at the master programme of Structural Geology and Tectonics at the Department of Geosciences, University of Oslo. When deciding to do a master thesis, I contacted Lars Eivind Augland at, Centre for Earth Evolution and Dynamics in the middle of August 2017. He proposed a thesis where the main goal was to look at extensional structures formed in Permian time in the inner Oslofjord, part of the Oslofield. I was intrigued by this topic as it would combine both field and laboratory work, in addition little work had been done on quantifying extension in the area.

Using the combined knowledge of structural geology and geochemistry gained through the years of study has been an exciting challenge. The thesis has also offered a steep learning curve when it comes to learning new softwares, interpreting, etc.

Fieldwork started in late August 2017 and was carried out until the middle of December 2017

Acknowledgement

First and foremost, I would like to thank my main supervisor Dr. Lars Eivind Augland and co-supervisor Dr. Anders Mattias Lundmark for the opportunity to write this thesis. The door to your offices have always been open for questions and discussions throughout the work on this thesis.

Furthermore, I would like to thank Gunnborg Bye Fjeld for guidance and help in sample preparation for the TIMS lab along with Salahalldin Akhavan who has helped in preparing thin sections.

I also wish to thank Einar Galtung Døsvig jr., harbourmaster at the Royal Norwegian Yacht Club for the help with launching the boat used during the fieldwork and for offering me a berth.

I must also take the opportunity to thank Michael Heeremans for providing med with previous mapping of the inner Oslofjord.

Finally, I would also like to thank my family and friends, especially Geir Dehli for valuable discussions and help during field work, this would not be possible without their encouragement and support. Thank you for keeping faith in me.

Thank you!
Nicolai Marthinsen

Contents

1 Purpose of study

The main task of this study is to quantify the amount of extension and displacement on faults which has occurred in the innermost Oslofjord, based on previous and new data collected from Huk, Nakkholmen, Lindøya, Hovedøya, Gressholmen, Bleikøya, Langøyene, Sjursøya, Husbergøya, Malmøyakalven, Malmøya, Ormøya, Ulvøya, Nordre Skjærholmen and Søndre Skjærholmen (fig 1.0).

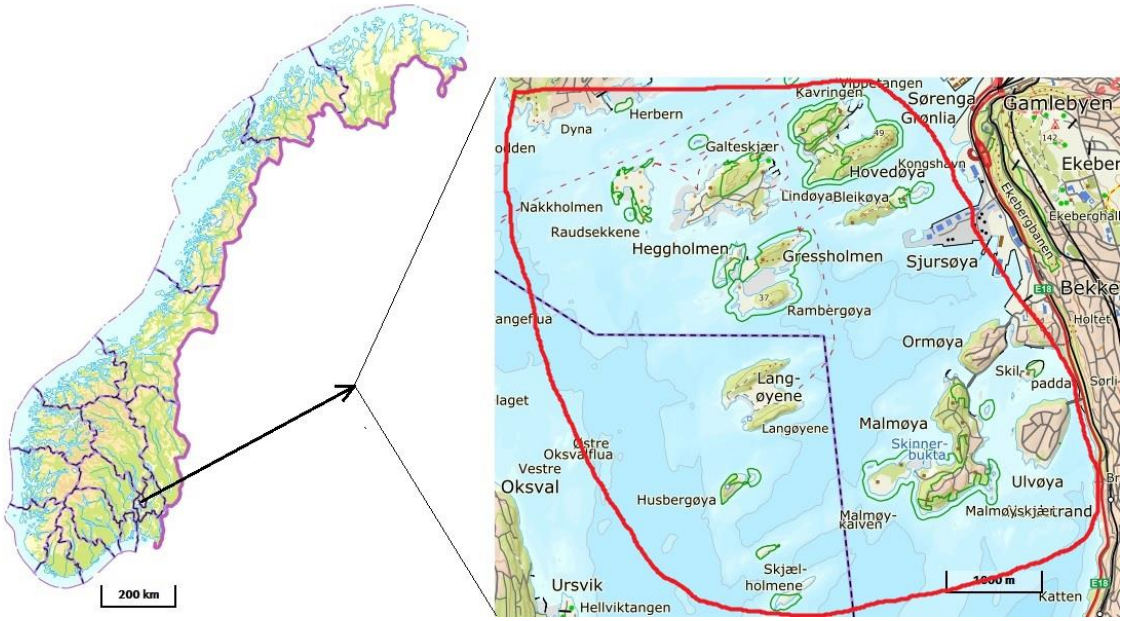

Figure 1.0: Map of Norway and a close-up map section of the study area within the red marking. Maps are taken from Norgeskart. The inner Oslo fjord is located just outside Oslo, the capitol of Norway.

The goals of this study can be broken down to four main tasks:

1. Map all Permian structures and make detailed geological maps where little or no previous work has been done.
2. Estimate the amount of displacement and extension using geometrical constraints based on the hinge zones from Caledonian folds and heave on faults displacing the stratigraphy.
3. Calculate the amount of extension associated with the intrusions within the study area,
4. Make a full-length profile across the whole study area from NW-SE and from the WSE-ENE to show the main structural styles in the area

2 Geological setting

Introduction

The study area is located in the south eastern part of Norway just outside the capital city Oslo (fig 1.0). It is part of the geologically well-known Oslo Field an area of around 10 000 km^2. The area extends approximately 115 km both north and south of Oslo to Lillehammer and Langesund respectively and varies in width from 40 to 70 km. Studies have placed Oslo at mid-latitudes during the Paleozoic Era. Oslo drifted rapidly towards the north during the Ordovician and during the Silurian Oslo was situated near the equator (Cocks and Torsvik, 2005; Bruton et al. 2010). The study area covers 24 km^2 of the total Oslo Region.

2.1 The lower Palaeozoic of the Oslo Region

The deposition of the lower Palaeozoic sediments visible in the Oslo Region took place in an epicontinental sea covering the Baltic Plate, ending up as a foreland basin at the foot of the Caledonian Orogeny (fig 2.1) (Bjørlykke, 1974; Larsen and Olaussen, 2005).

According to Larsen and Olaussen (2005) the basin fill of the Oslo Region can be divided into four phases. The first phase is characterized by a shallow southward transgressing sea, during Early to Middle Cambrian. The second phase, Late Cambrian to Middle Ordovician, characterized by low sedimentation rate which is common for an epicontinental sea. Shallow marine warm water carbonates along with silt and sandstones are typical in the third phase, which is linked to the onset of foreland basin formation during Late Ordovician into lower part of late Silurian. The last and final event is the foreland alluvial basin fill during Late Silurian (Larsen and Olaussen, 2005).

During Cambrian age, the sea level started to rise and most of Norway and Baltica were flooded. This flooding led to a shallow sea with low sedimentation rate, resulting in deposition of sandstone and conglomerate during early Cambrian in the northern part of the Oslo Region. During the middle and upper Cambrian thin layers of organic rich Alum shale was deposited along with black mudstones and thin limestones, due to the calm and shallow waters (Larsen and Olaussen, 2005; Nakrem and Worsley, 2008).

In Ordovician time we find one of the highest global sea levels recorded. The high sea level along with a relatively flat surface developed typical epicontinental sea sedimentation, with repeating sedimentation of mudstone and limestone (Bjørlykke, 1974; Brenchly and Newall, 1980). During the lower and middle Ordovician the water circulation increased, and slightly greyer mudstone developed with nodular limestone along with massive limestone and gray/black shale. In the middle Ordovician the depositional environment varied a lot across the Oslo Region. Massive limestones were deposited in the North, South and Western part, and more shale and nodular limestone in the Oslo-Asker district (Larsen and Olaussen, 2005; Nakrem and Worsley, 2008). Sediment composition and depositional environment changed in the Upper part of Ordovician and shows a continuing regression to the Ordovician/Silurian Boundary. It differs from middle Ordovician with coarse sandstone and limestone. There was also a higher sedimentation rate in the upper Ordovician. Thick and thin bedded calcareous and siliciclastic sandstones dominate the Uppermost part of Ordovician. Channels with varying grain size and conglomerates are found within the Uppermost sequence (Bjørlykke, 1974; Brenchly and Newall, 1980; Larsen and Olaussen, 2005).

In the Early Silurian a rapid transgression occurred, leading to increasing sea level depths in the Oslo Region. Dark muds, thin layers of sand and silt along with calcareous mud were deposited in the Oslo area, from surrounding shallower areas. With the increasing sea level and subsiding highs, a sedimentary succession mostly consisting of marine shales originating from mud accumulated in the foreland trough that was being formed. The rise in sea level and subsidence was followed by a gradual uplift in Late Silurian. The gradual uplift led to a transition to shallow marine limestones in the Oslo Region. As the Caledonides continued to rise a distinctive change between siliciclastic sediments and carbonates occur. This distinctive change shows a transition to a non-marine and red-bed facies foreland basin fill ahead of the SE-propagating thrust front, with occasional tidal channels. (Worsley et al. 1982; Larsen and Olaussen, 2005; Nakrem and Worsley, 2008).

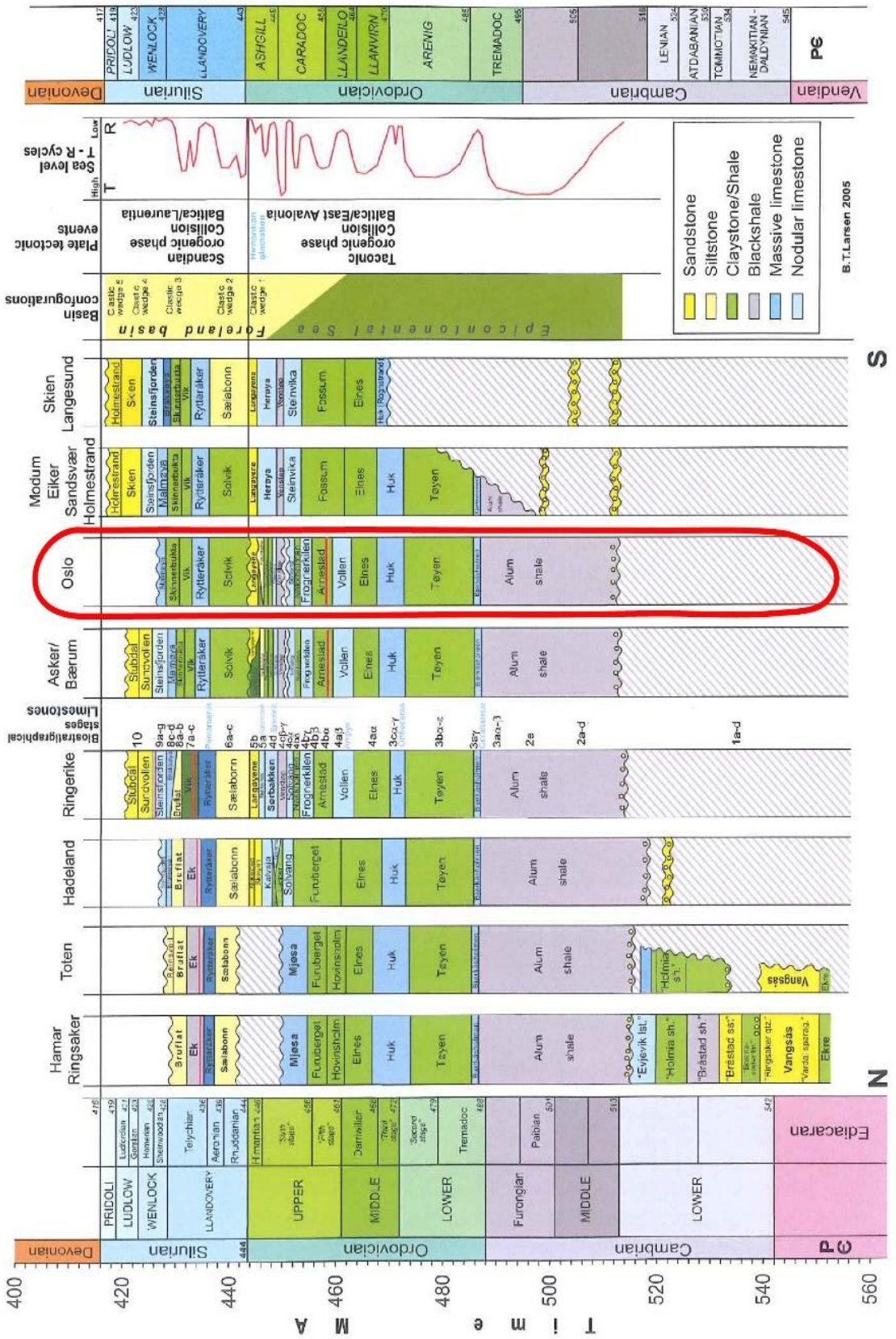

Figure 2.1: Stratigraphy of Lower Palaeozoic in the Oslo Region, with the study area inside the red marking. Figure modified from Larsen and Olaussen (2015)

2.2 The Scandinavian Caledonides

The Scandinavian Caledonides formed as a response to the continuous convergence of the Baltican and Laurentian plates that led to collision and closing of the Iapetus Ocean, along with subduction of the Baltic margin underneath Laurentia during Silurian to Devonian time (fig 2.2) (Roberts, 2003). As a response to the collision of the two plates sequences of nappes were emplaced on top of the subducted Baltican plate, divided into five main units (Roberts and Gee, 1985; Hurich et al. 1989; Roberts, 2003; Korja et al. 2008).

1) The Autochthon – Parautochthon
2) The Lower Allochthon
3) The Middle Allochthon
4) The Upper Allochthon
5) The Uppermost Allochthon

The Autochthon - Parautochthon consist of sedimentary rocks with a slightly westward dip deposited prior to or in front of the orogen. A weakly metamorphosed sedimentary sequence makes up the Lower Allochthon deriving from the Baltic margin. The Middle Allochthon shows more signs of metamorphism than the Lower Allochthon and consists mainly of Precambrian rocks also deriving from the Baltica margin. The Upper Allochthon varies greatly in the degree of metamorphism from lower to upper amphibolite facies and in some places even eclogite facies. The rocks that make up this unit are mainly derived from the oceanic crust from the Iapetus Ocean. The Uppermost Allochthon is exotic, probably remnants of Laurentia (fig 2.3) (Andersen, 1998; Roberts, 2003; Korja et al. 2008).

The general transport direction of the Caledonian nappes shows an east to south-east direction. But the Oslo Region stands out from the generally interpreted east to south-east transport direction, having a more south south-east direction (fig 2.4) (Hossack and Copper, 1986; Fossen et al. 2008; Bruton et al. 2010).

Collisional events through the Silurian to Devonian age have resulted in the formation of the Scandinavian Caledonides. Roberts (2003) defines the Scandian event in Mid Silurian to Early Devonian to be the principal event for emplacement of allochthons in Norway. The

period is recognized by the collision between the Baltic and Laurentian plates, leading to the subduction of the Baltic margin beneath Laurentia (Gee, 1975; Roberts, 2003). Following these events there was a major collapse related extensional event in the Middle to Late Devonian about 400 Ma. When the contractional forces seized, back sliding of the deposited nappes due to gravity continued until they reached a point of equilibrium (Korja et al. 2008; Gee et al. 2008).

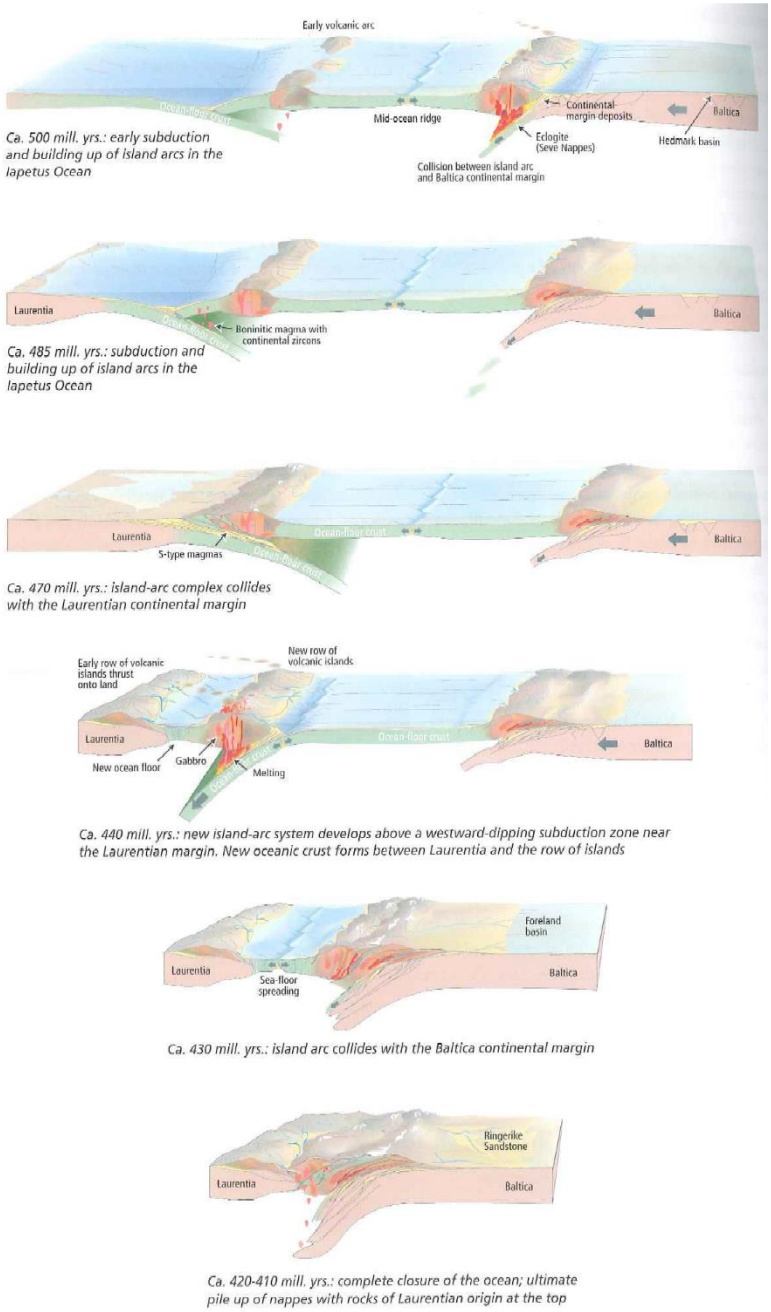

Figure 2.2: A modelled evolution of the Caledonian mountain belt, from the beginning of convergence of the Baltica and Laurentian plate till the full closure of the Iapetus ocean. From Fossen et al. (2008).

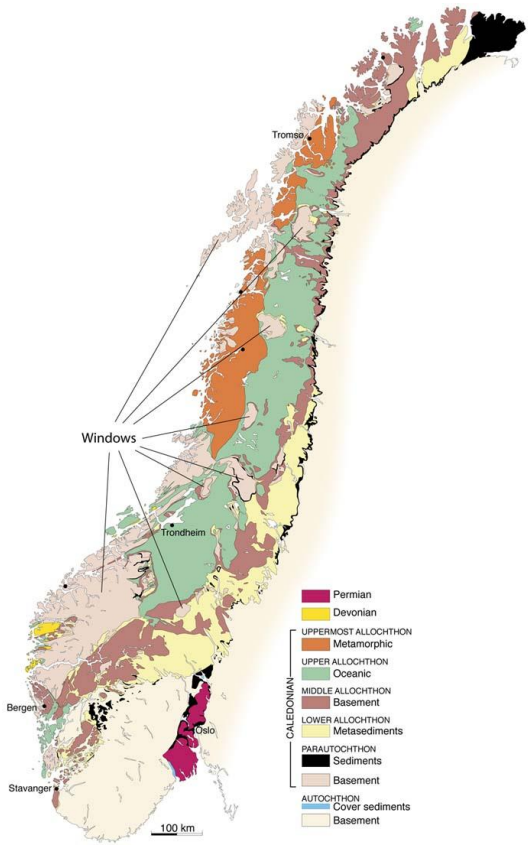

Figure 2.3: Main geological units of the Scandinavian Caledonides. From Fossen (2010).

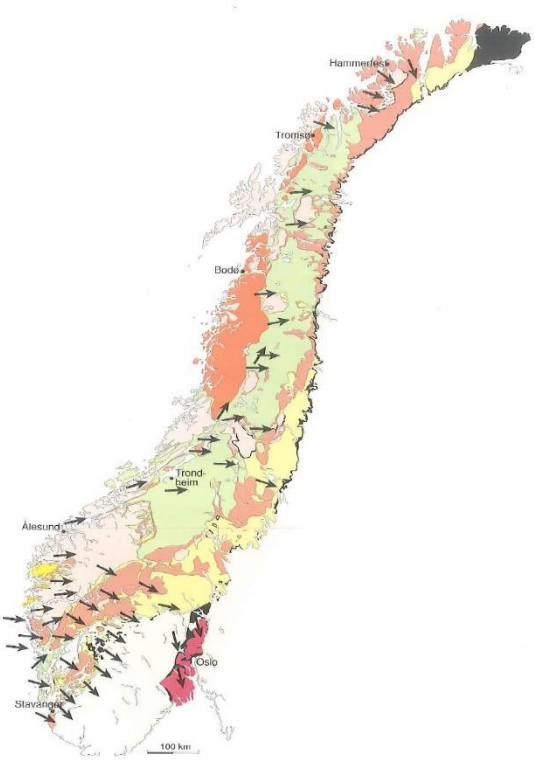

Figure 2.4: The principal lineation orientation of the Caledonides. The overall transport direction to the east south-east, but in the Oslo Region the transport direction is more south south-east. From Fossen et al. (2008).

2.2.1 Structures following the Caledonian collapse and extension

The Oslo Region is located in the Osen-Røa Nappe Complex within the Lower Allochthon in the frontal zone of the Caledonian Nappe System (Nystuen 1981; Bruton et al. 2010). The Lower Palaeozoic sediments deposited in the Oslo Region have undergone deformation in varying degree. Deformation has been controlled by the transport length in the south and southeast direction, and within the nappe pile deformation has been controlled by lithology and thickness of the units (Morley, 1986a, 1986b, 1987, 1994; Bruton et al. 2010). Structural orientation also varies within the nappe of the Oslo Region, with ENE-WSW being the dominant orientation, but locally in the Oslo area, NE-SW oriented structures are also found (Bruton et al. 2010).

Bruton et al (2010) has divided the structural evolution the Caledonides in the Oslo Region into four levels based on structural characteristics.

1) **The basal thrust system**
   Within the Cambrian Alum Shale Formation, we find the Osen-Røa thrust/detachment, which underlie the sedimentary rocks of the allochthonous/parautochthonous unit (Harper and Owen, 1983; Bruton et al. 2010). From the main Osen-Røa basal-thrust, faults propagate upwards in the direction of transport developing imbricate fans, duplexes and folds (Bruton et al. 2010). It has been proposed by Morley (1986a) that the Osen-Røa basal thrust dies out in the Holmestrand Langesund area.

2) **The middle thrust system**
   Generally strain intensity decreases upwards over the basal thrust, but the Lower Palaeozoic succession in the Oslo Region shows great deformation throughout (Morley, 1986b, 1994). The style of deformation changes upwards through the Cambro-Silurian stratigraphy from imbricate thrusts, triangle and pop-up zones and buckled folds (Morley, 1986b).

3) **Level 3**
   The thrusts within level 3 are most likely linked with the upward propagating faults of level 2 (Bruton et al. 2010).

4) **Level 4**
   As for the next, level 4 master faults are closely linked to the faults of level 3. They

only appear in some areas, where they have penetrated the Ringerike Group sandstones (Bruton et al. 2010).

Within the Oslo Region two main types of folds can be recognized; 1) thrust related folds and 2) buckle folds. Thrust related folds are most common within the Cambro-Ordovician rocks where the geometry is controlled by the fault strain. Buckled folds are found stratigraphically above the thrust related folds. They often form fold trains, meaning folds of similar wavelength and orientation (Morley, 1986b).

2.3 The Carboniferous and Permian

Following the Caledonian mountain building and folding and thrusting, weathering and erosion of the Caledonian mountain took over as dominant processes. No distinct geological process apart from the erosion is preserved in the Oslo Region between Late Silurian to Late Carboniferous (Larsen et al. 2008a). Two major tectonic models have been proposed for the formation of the Oslo Rift, the first associates its formation to post-Variscan tectonics and the second to the emergence of a mantle plume

McCann et al (2006) and Ziegler et al. (2006) have described the post-Variscan tectonics as a principally NW-SE striking fault system in western Europe. The Sorgenfrei-Tornquist Zone with the Tornquist dextral strike slip fault is the northernmost and largest fault system of post-Variscan age (fig 2.5).

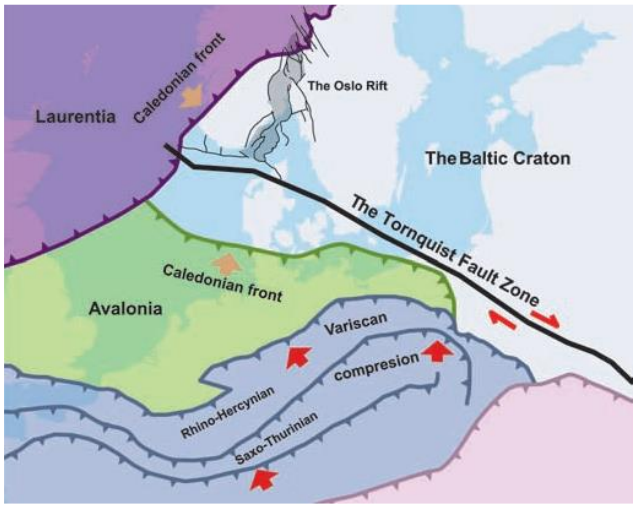

Figure 2.5: Western Europe with the Tornquist fault zone and Oslo rift. From Larsen et al. (2008b).

According to this model, extensional stress in relation to the strike-slip faulting led to rifting throughout the zone (Heeremans et al. 1997). From inside the Variscan orogen to the foreland rifts were formed, with the Oslorift considered the largest and furthest to the north (Larsen et al. 2008b).

Another model proposed for the development of the Oslorift after Ro and Faleide (1992) is the event of a mantle plume (fig 2.7). Increasing temperatures in the asthenosphere resulted in uplift due to the thermal expansion of the lithosphere. This melting of the asthenosphere along with intruded melt in the lower crust resulted in uplift and erosion of the rift zone.

The time of highest tectonic and magmatic activity in the Oslo Rift was after the onset of the rift during Late Carboniferous to Early Permian (Sundvoll et al. 1990; Heeremans et al. 1997; Corfu and Dahlgren, 2007). The architecture of the Oslo Rift has been compared to the Kenya Rift of East Africa, an active high volcanic continental rift (Larsen et al. 2008a, 2008b).

2.3.1 Evolution of the Oslo Rift

The Oslo Graben is approximately 220 km long with an average width of 60 km, made up of the Akershus and Vestfold graben segments (fig 2.6) (Larsen et al., 2008b) and its development has been divided into six stages.

1. Initiation of the Oslo Rift began in Late Carboniferous time recognized by sediment depositions in the southern parts of the Oslo Graben. This sedimentation led to the development of the Kolsås and Tanum formations, consisting of red mudstones and sandstones with adjacent conglomerates. These are overlain by the Skagum Formation, which include volcanic debris and completes the Asker Group (Larsen et al. 2008b).

2. Basaltic lava flows dominate stage two of the rift development, with a wide spectre of composition. (Larsen et al. 2008b).

3. The basaltic lava flow continued into stage three but with less intensity. This was the time of highest tectonic and magmatic activity and the first eruptions of rhomb porphyry lavas was during stage three. During this stage eruptions were intensified covering vast areas with rhomb porphyry (Larsen et al. 2008b).

4. Stage four of the rift development is marked with basaltic central volcanoes across the rift. Rhomb porphyry lava eruptions decreased and large faults bounding the grabens have now been developed (Larsen et al. 2008b).

5. The development of large batholiths in the inner Vestfold and northern parts of Oslo is part of stage five (Larsen et al. 2008b).

6. Stage six marks the termination of the rift development, recognized by granitic / syenitic intrusions in two separate events respectively in Tryvann and Hurdal (Sundvoll et al., 1990; Larsen et al. 2008b).

NNW-SSE oriented faults and dikes dominate throughout the Oslo Graben. Signs of both ductile and brittle deformation is found in the Precambrian rocks and faulted rocks within the Oslo Graben (Ramberg et al. 1977; Larsen and Olaussen, 2005). The Oslofjorden Fault Zone developed during stage three of the rift development, bounds the Vestfold Graben to the east and west and its displacement is estimated to approximately 3 km.

(Ramberg and Larsen, 1978 in Larsen and Olaussen, 2005; Neumann et al. 1992; Larsen and Olaussen, 2005).

Another factor contributing to the development of the Oslo Rift is the increased heat flow from high crustal temperatures (fig 2.7). The lithosphere had already weakened from the increased temperatures at the depth (Larsen et al. 2008a). The series of half grabens that make up the Oslo Graben have been interpreted as faults becoming more listric with depth based on seismics. (Neumann, 1992).

The pre-rift sediments of Lower Palaeozoic are preserved throughout the Oslo Graben because of downfaulting and vary in thickness from approximately 2 km to 5 km. (Ramberg and Spjeldnæs, 1978; Ro and Faleide, 1992).

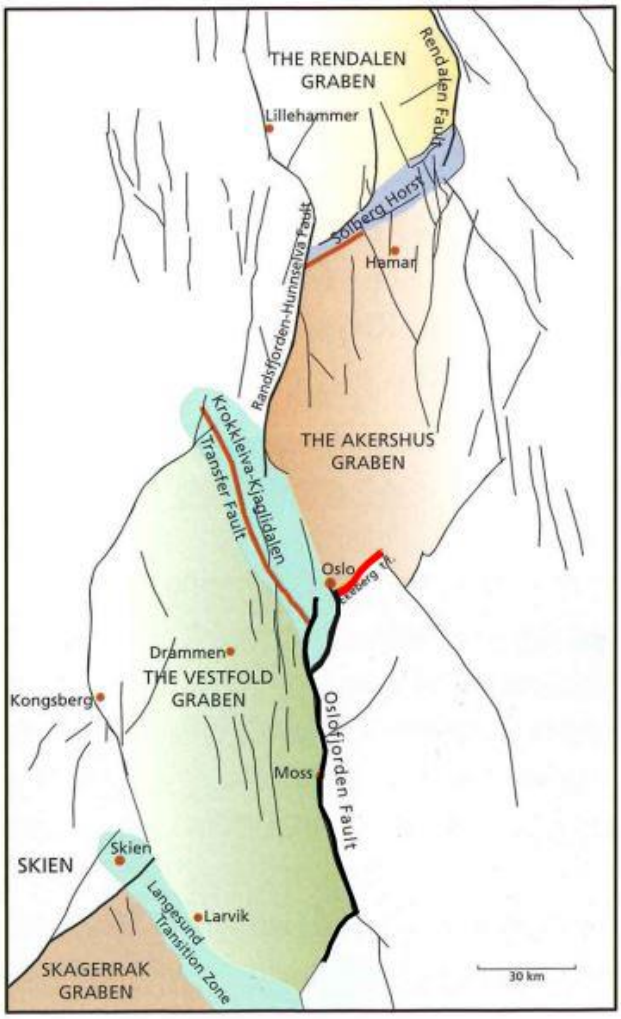

Figure 2.6: The graben segments that make up the Oslo Graben with the major faults highlighted, Oslofjorden Fault in black and the Ekeberg Fault in red. Modified from Larsen et al. (2008b).

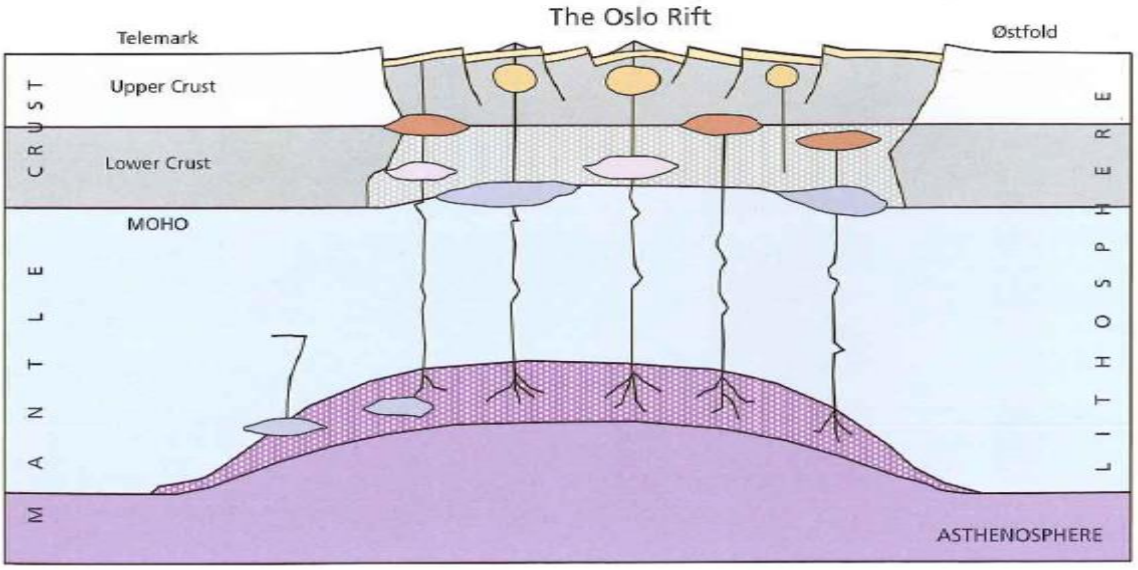

Figure 2.7: The Oslo Rift showing lithospheric thinning due to increased temperature in the crust and at the base of the lithosphere. From Larsen et al. (2008a).

3 Material and methods

Introduction

The different softwares and methods used in the study will be presented in this chapter. Field work has been the primary method of data gathering for this thesis, consisting of measuring and recording structures of interest, sketching and sample collecting for the possibility of geochemical/chronological analyses. A total of 9 thin sections were made from the intrusions across the study area. Mineral separation was performed on two samples respectively from Malmøya and Gressholmen to attempt U-Pb dating of z*ircons*. The main results of the fieldwork are shown in the form of a digitized map of the whole study area.

3.1 Material

Strike and dip measurements on faults, bedding, intrusions and lineations was made using a *Silva Expedition S compass*. The right-hand rule was applied to all measurements, meaning that the dip of the surface would always be to the right of the measured strike direction. Previous mapping of the area by Brøgger (1885), Dehli (2012), Repshus (2012) and by students in the GEL2150 course were used as background data for the fieldmapping.

3.2 Software

The digitalization of the field maps was done by the open source software *Quantum Geographical Information System – Qgis*. This program allows the user to edit georeferenced maps, adding geological formations, structures and display orientation of the different structures measured in field.

Adobe Illustrator was used to make the geological cross sections. The topography along with geological formations of the desired area was exported from *Qgis* and edited in *Adobe Illustrator* to make cross sections.

Visualization and processing of strike and dip measurements from the field work was performed using the software *GeoOrient* (Holcombe, 2011) version 9.5.1. This software makes it possible to display the strike and dip recorded and calculate the general fold axis (β-axis) and axial plane.

3.3 Field work

Field work was carried out on 13 different localities between the end of August and middle of December 2017. Most of the field area was only accessible by boat. The larger islands were, covered by the ferry service of Oslo municipality, but for the outermost islands a private boat was used. Private properties and developed infrastructure made field work somewhat difficult on some of the islands.

The days spent in the field were used to walk around the islands following the shoreline where outcrops and structures were most visible. Recordings of Permian structures such as extensional faults with lineations where visible were made along with recording of intrusions. Recordings included strike and dip measurements using the right-hand rule and the width of the intrusions were recorded by the help a folding ruler.

3.4 Lab work

From the samples collected in field 9 thin sections was made. This was done by cutting the sample to a size of approximately 2,5 x 2,5 cm on a diamond saw. The cut sections were then passed on to Salahalldin Akhavan at the Department of Geosciences, University of Oslo to be grinded and polished down to a thickness of only 30 µm glued to a microscope glass slide. This process made it possible to study the mineral content of all the sample rocks under plane and crossed polarized light. The samples collected, and their intended use are displayed in table 3.1.

The two samples collected from Gressholmen and Malmøya believed to be lamprophyres underwent crushing and mineral separation to attempt U-Pb dating of suitable minerals (fig 3.1).

First the samples were crushed to a grain size of approximately 0,5 cm in the *Jaw Crusher*, and then again using the *Retsch Crusher* ending up with a fined grained powder with a size of 0,5 mm. Crushed material was then washed by the help of a *Wilfley table* to separate the lighter material and dust from the heavier material. The separated material was then left to dry in an oven before being sieved to the desired grain size. The remaining grains then underwent magnetic separation several times at different ampere, separating the magnetic grains from the non-magnetic grains using the free fall method. The non-magnetic grains were then separated

using heavy liquid, *diiodmethane*, with a density of ρ = 3,2-3-3. This would make mineral of interest, mainly *zircon*, sink to the bottom, while the lighter material would float to the surface. The heavy material at the bottom was then drained out and sent through the Frantz isodynamic separator for a last magnetic separation. Finally grains of what was believed to be zircons were picked using tweezers under a microscope.

The next step before analyses was abrasion. This process starts with annealing at 900 °C for ca. 72 hours followed by chemical abrasion in HF+ HNO_3^-, for ca. 14 hours at 195 °C, to remove domains of the zircons that has experienced Pb loss.

Unfortunately, after the abrasion process it was obvious that there was no zircon in the two collected samples.

Table 3.1: List of samples collected and their locations within the study area.

Collected Samples					
Sample nr:	Name of island:	Locality:	Geochronolgy:	Thin section:	Type:
0.1	Gressholmen	Loc 1.11	X	X	Lamprophyres
0.2	Gressholmen	Loc 1.16		X	Syenite
0.3	Hovedøya	Loc 2.1		X	Syenite
0.6	Hovedøya	Loc 2.20		X	Syenite
0.9	Bleikøya	Loc 3.7		X	Syenite
1.1	Nakkholmen	Loc 4.19		X	Rhomb porphyry
1.9	Lindøya	Loc 5.3		X	Syenite
1.10	Malmøya	Loc 11.1	X	X	Lamprophyres
1.11	Malmøya	Loc 11.4		X	Syenite

Figure 3.1: Lab equipment used for mineral separation. A) Jaw Crusher, B) Retsch Crusher, C) Wilfley table, D) Free fall magnetic separation, D) Heavy liquid separation, F) Frantz isodynamic separator.

3.5 Construction of profiles and calculations of displacement

The following section will give a detailed description on methods and calculations used to construct cross sections and calculate the amount of vertical displacement across faults.

3.5.1 Cross section calculations

When constructing the cross-sections, the apparent dip had to be calculated where the strike of the geological formations was not perpendicular to the cross-section line. This was done by equation 3.1.

$$tan(\alpha_{Apperent\ Dip}) = \tan(\alpha_{TrueDip}) \times \sin(\alpha_{Strike} - \alpha_{Profile})$$

Equation 3.1: Equation used to calculate apparent dip, from Groshong (2006)

3.5.2 Vertical displacement calculations

For vertical displacement calculations between islands and normal faults within each islands the following steps were used.

1. Measure the map distance between the intersection of the fold axis and the cross-section line on the two islands of interest, A and B (fig 3.2).
2. Find corresponding hinge points on the two islands using the cross-sections.
3. Extrapolate the hinge point from the cross-section on island A to the cross-section on island B using the plunge of the fold axis (equation 3.2; figure 3.3).
4. Compare the extrapolated position of the hinge line on island B to the observed position of the hinge line, or if not exposed, to the inferred position of the hinge line from the cross-section on island B. The difference represents the vertical displacement between the two cross-sections.

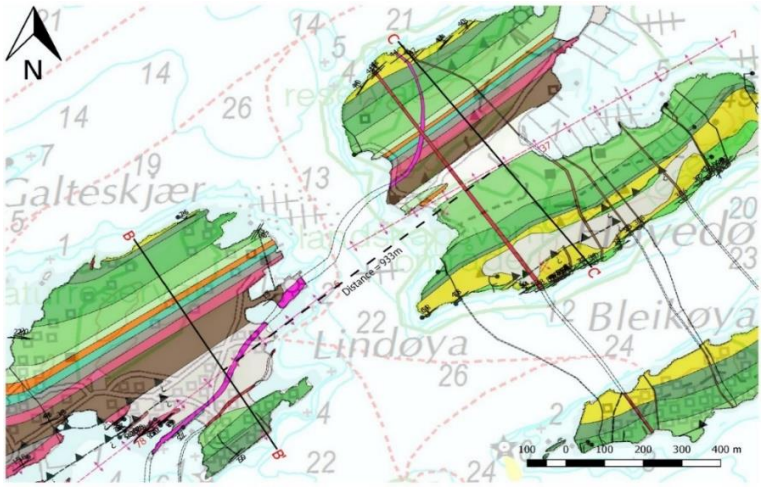

Figure 3.2: Example of step 1, measuring distance between cross-section lines perpendicular to the trend of the hinge line. The distance in the example was measured to 933 m.

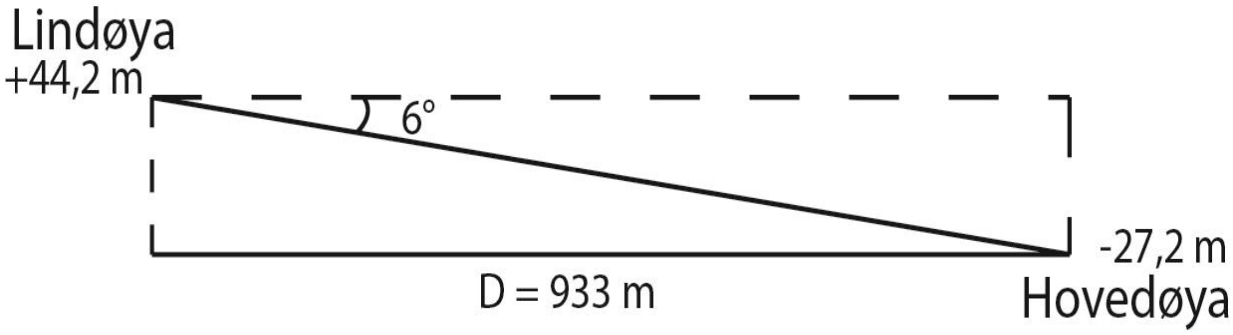

Figure 3.3: Example of values extracted from map and profiles used to calculate theoretical position of a given formation boundary if there was no displacement.

$$\tan A = \frac{a}{b} \rightarrow a = \tan A \times b$$

Equation 3.2: Trigonometric formula used to calculate extension across islands and extensional faults.

If the fold axis on one of the two islands to be calculated was not visible a geological formation boundary was chosen. The strike direction of the chosen geological formation was then extrapolated across to the neighbouring island. Then the distance from the extrapolated line to the correct geological formation, i.e. the heave was measured (fig 3.5). With the measured value and the calculated mean dip from the geological formation an approximate displacement was calculated (fig 3.4 and equation 3.2). This method assumes vertical displacement on the faults.

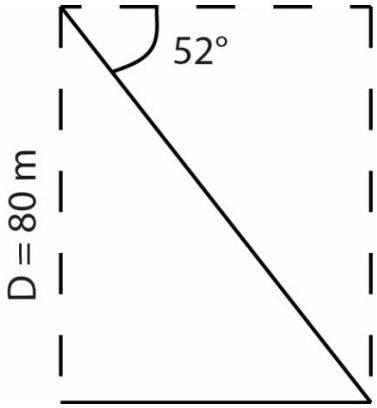

Figure 3.4: Example of values extracted from map used to calculate theoretical displacement between two islands, where one island is missing a fold limb.

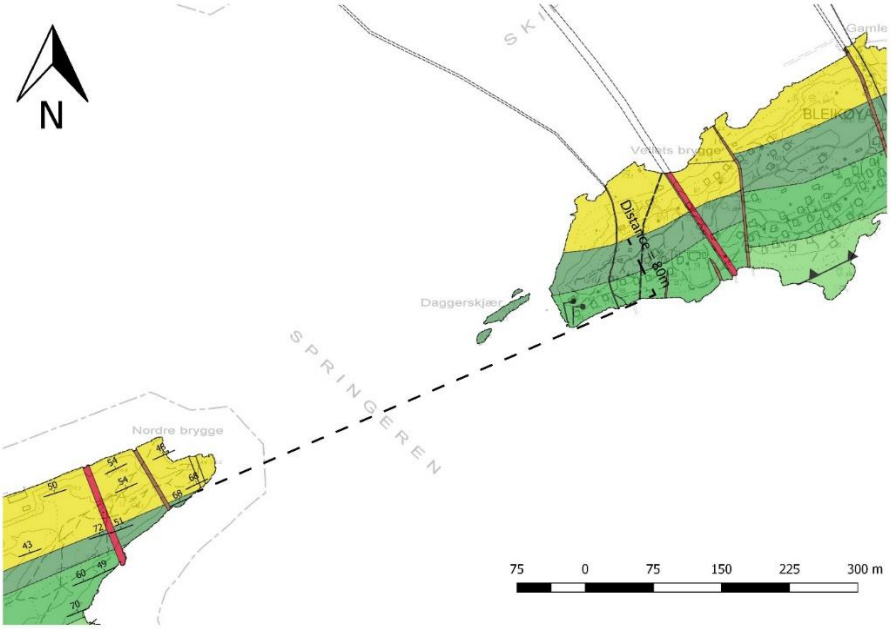

Figure 3.5: Example of the method used to calculate the approximate displacement between two islands, when one island Is lacking a fold axis. The horizontal distance (heave) in the example was measured to 80 m.

A final method, which also acted as quality check to the previous calculations was to measure the amount of displacement straight from the profiles created. This was done by finding the dip on both sides of a fault or where the angle of dip changed with more than 15 degrees, across dikes. A protractor was then used to find the corresponding dip angels in the profile. The length between the two points would then give the approximate amount of vertical displacement (fig 3.6). This method assumes that the fold geometries have been accurately reconstructed.

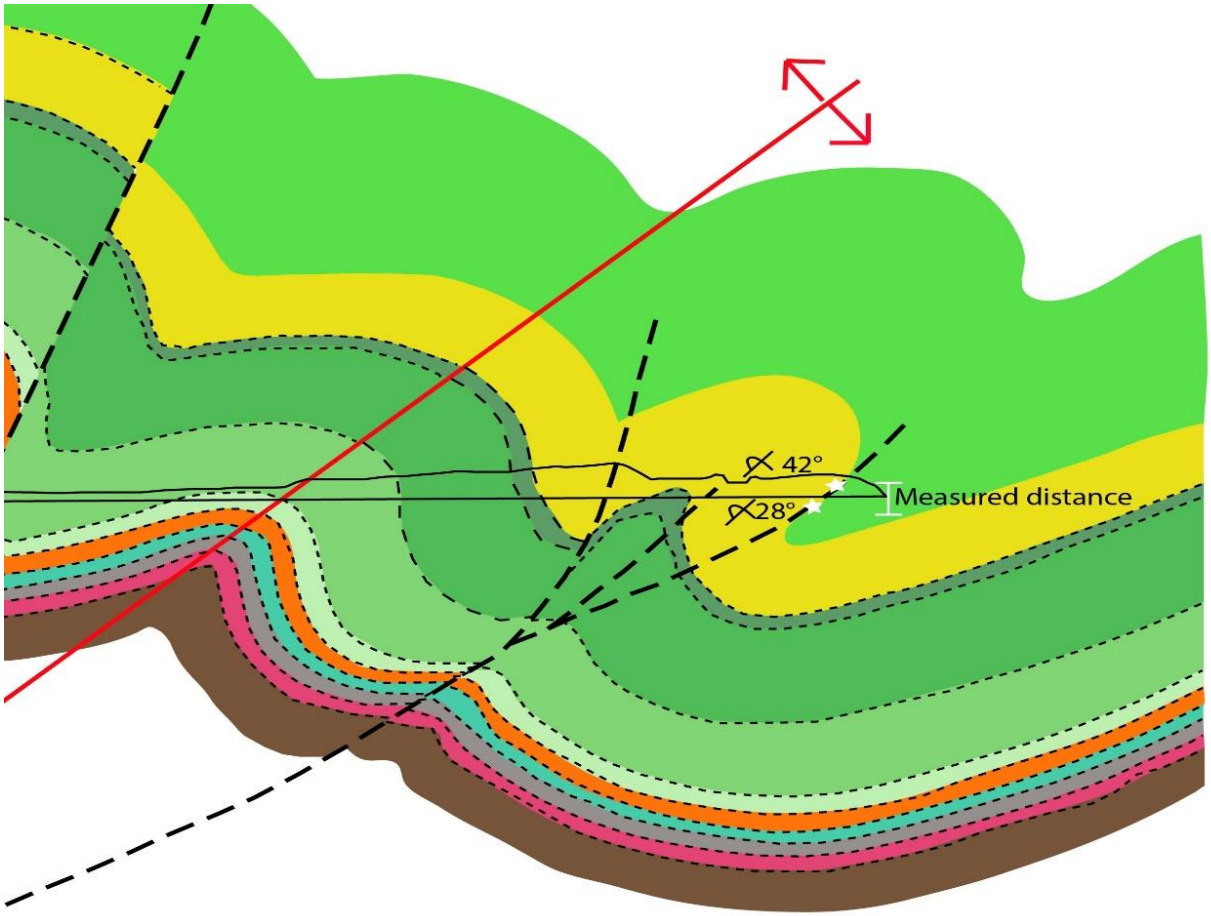

Figure 3.6: Example of how overturned bedding readings from the map is located in the profiles marked by "white stars" to estimate the amount of displacement. Profile modified from Repshus (2012).

4 Terminology

Introduction

The geological structures that are studied and mapped throughout the study area will be explained shortly in this section.

4.1 Folds

Folds develop as planar structures that are squeezed to curved structures during ductile deformation. If the geometry of the fold is repeated along the axial trace the fold is said to be harmonic. If this is not the case and the wavelength and geometry varies the fold is disharmonic. The area of highest curvature on a fold is at the centre of the hinge zone and referred to as the hinge point. The axial surface together with the hinge line can tell us about the orientation of a fold. If the limbs of the fold dip away from the hinge zone it is called an antiform and the opposite for a synform. These two terms change names to anticlines and synclines when stratigraphy is known, where for anticlines the stratigraphy gets older towards the axial surface trace and for synclines the stratigraphy gets younger towards axial surface trace (fig 4.1) (Fossen, 2010a).

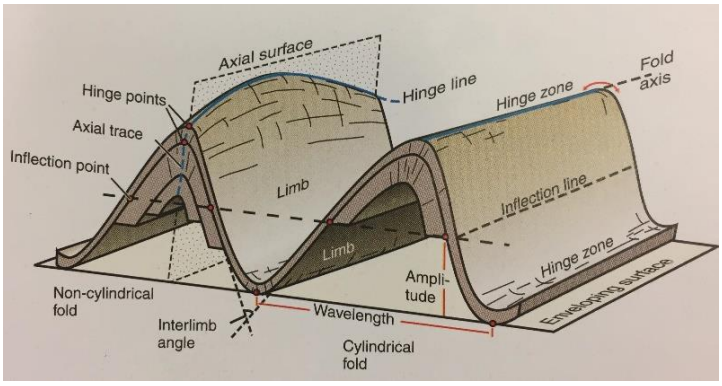

Figure 4.1: Detailed description of a fold. From Fossen (2010).

4.2 Normal faults

Extensional faults are recognized by extension of the crust or for example extension visible in geological formations, with one lithology either moved up or down in accordance to a reference point. This is shown in (fig 4.2, b), a dip-slip fault where the displacement is almost the same as the thickness of the layers. To be able to classify the fault as an extensional fault the distance between two reference points on both sides of the fault must increase under deformation and the extension must be perpendicular to the strike of the fault (Fossen, 2010b).

The amount of dip on a fault is very important as seen in (fig 4.2) normal faults vary all the way from vertical (fig 4.2, a) to horizontal (fig 4.2, b). Neither the vertical or horizontal fault will display any extension they will not show any change in length perpendicular to the fault (Fossen, 2010b).

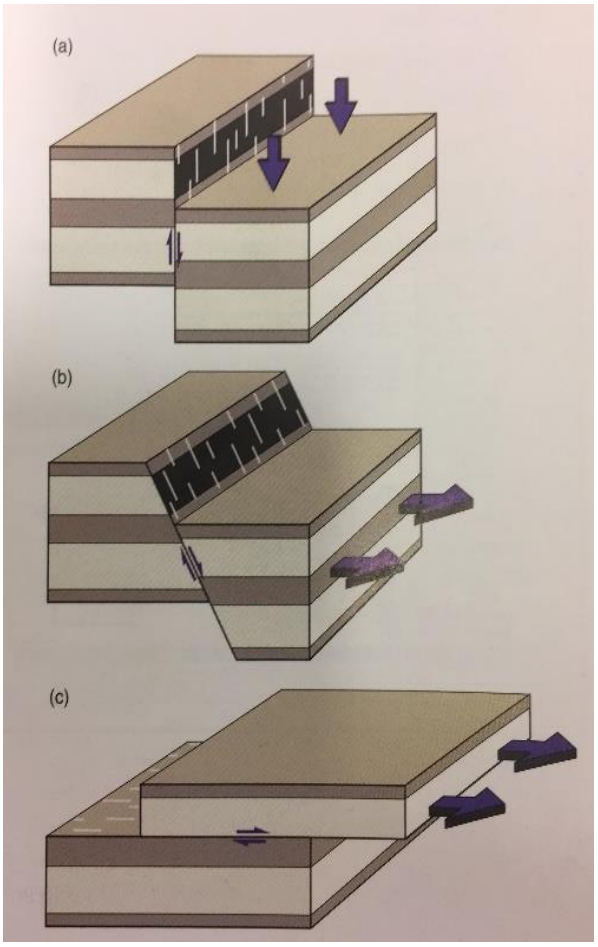

Figure 4.2: Displays variations of normal faults from a) vertical fault, b) extensional fault, c) horizontal fault. From Fossen (2010).

Most extensional faults have a dip of ca. 60°, but this is not always the case. Low angle extensional faults also exist. An explanation for this might be the reactivation of earlier thrust faults or rotated high angel extensional faults. In the same way steep faults may be the result of reactivated joints or strike-slip faults. But in some cases, low and high angle faults are formed without any prior weak zones (Fossen, 2010b).

4.3 Intrusions

Intrusive rocks are made from crystallized magma in the Earth's crust. Magmatic intrusions that cut through already existing strata are known as dikes. Magma cools down slowly within the Earth's crust which gives more time for minerals to grow. Dikes on the other hand are less coarse than plutonic rocks and known as hypabyssal/sub volcanic rock. Igneous rocks may also have varying grain size, where the larger crystals are known as phenocrysts varying in size from a few millimetres to a couple centimetres with a surrounding matrix which is often fine grained. The finer grained matrix together with phenocrysts makes up the distinct porphyry rocks (Dutrow and Klein, 2008).

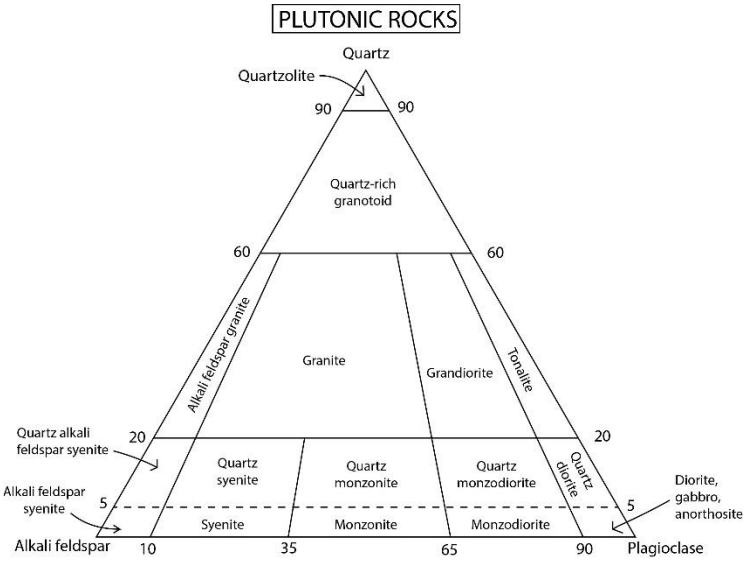

Figure 4.4: Classification of plutonic rocks based on quartz, alkali feldspar and plagioclase content. Modified from Dutrow & Klein (2008).

Variations in chemical compositions differ, with the biggest variations occurring in the SiO_2 and Al_2O_3 components. Rocks formed by magma low in SiO_2 are called mafic rocks and will often be dark because of the high content of ferromagnesian minerals. When the SiO_2 content is high, less ferromagnesian minerals will be present, giving the rock a lighter colour compared to the mafic rocks and is called felsic rocks (fig 4.4) (Dutrow and Klein, 2008).

5 Results

Introduction

The study area is made up of sediments from Middle Ordovician to Lower Silurian age. The sediments are folded by into a series of SE verging anticlines and synclines throughout the with fold axes trending in a roughly NE-SW direction, with some of the limbs being overturned. The folds are associated with compressional faults and duplexes. Roughly N-S tending extensional faults and dikes postdate the compressional folds and faults.

5.1 Stratigraphy of the study area

Below, the different formations (fig 5.1) present in the study area are briefly described based on Owen et al (1990), Brenchley & Newall (1975), Baarli (1985) and Worsley et al (1983). The formations below the lowest outcropping formation in the study area, the Elnes Formation, are not described in detail below, but are included in fig 5.1. The same is the case for the formations above the uppermost outcropping formation in the study area, the Malmøya Formation.

The oldest formation mapped within the study area is the *Elnes Formation. It* is a shale dominated formation with increasing shale content towards the upper boundary. From the base upwards, limestone beds and weathered nodular limestone are present but decrease towards the top of the formation. The thickness of the formation is estimated to approximately 60 m (Owen et al. 1990).

The *Vollen Formation* is recognized by alternating beds/nodules of limestone, interbedded with calcareous shale. No complete section of this formation is found within the study area, but approximately 40 m of the base is exposed at Bygdøy due to faulting (Owen et al. 1990).

The overlying *Arnestad Formation* consists of dark shales with thin limestone horizons. The horizons vary in thickness from approximately 30-40 cm, while the horizons of nodular and bedded limestone never exceed more than 10 cm. The Arnestad Formation is estimated to a thickness of 22-45 m (Owen et al. 1990).

The base of the *Frognerkilen Formation* is marked by a clear transition from shale dominated succession of the Arnestad Formation to fragmented limestones. Towards the top of the

Frognerkilen Formation a shifting layering of nodular limestone and shales is seen, respectively 10 cm and 35 cm thick layers (Owen et al. 1990).

The lower part of the *Nakkholmen Formation* is recognized by thick dark shales along with black ellipsoidal limestone nodules at some levels throughout the formation. Pyrite nodules may also be found within the formation and the formation various in thickness from approximately 3040 m to only 12-13 m (Owen et al. 1990).

The *Solvang Formation* is a limestone dominated unit with varying amount of interbedded calcareous shales. The boundary between the Nakkholmen and Solvang Formations is recognized by the occurrence of conspicuous pyrite bands, or at the last thick shale of the underlying Nakkholmen Formation (Owen et al. 1990).

The *Venstøp Formation* is defined as a dark shale, with the lower and upper boundary marked by pale coloured limestones. In the Oslo Region the top of Venstøp Formation is recognized by planar limestones and at the base a thin phosphorite conglomerate (Owen et al. 1990).

The upper boundary of the *Grimsøya Formation* consists of alternating limestone beds, shales and in some places beds of siltstone. The lower boundary is made up of nodular limestone with signs of weathering shale giving the shale a rusty colour in some places (Owen et al. 1990).

The *Skjerholmen Formation* is made up by light grey calcareous beds of shales with signs of weathering together with calcareous siltstones, fine calcareous sandstone and nodular silty limestones. The transition between Grimsøya and Skjerholmen Formations can be seen where the first thick shale of the Skjerholmen Formation overlies the nodular limestone of the Grimsøya Formation (Owen et al. 1990).

The lower part of the *Skogerholmen Formation* can be recognized by a transition to a limestone dominated unit, differentiating it from the shale dominated Skjerholmen Formation. The formation various in thickness from 33-43 m (Owen et al. 1990).

The *Husbergøya Formation is* described by Brenchley & Newall (1975). The lower most part displays a transition from nodular limestone to a shale dominated succession. Calcareous sandy horizons with increasing intervals towards the top of the formation is common. The upper 5m of the formation is recognized by bedded brown weathered sandstone. The

formation has an estimated thickness of 10-35 m (Brenchley & Newall, 1975; Owen et al. 1990).

The *Langøyene Formation* is made up by shales, laminated sandstones and thin limestones overlying the brown weathered sandstone of the Husbergøya Formation. The Langøyene Formation varies a lot, from calcareous sandstone, shale and thin limestone layers to breccia, but it is dominated by sand. The formation is estimated to a thickness of approximately 1-60 m (Brenchley & Newall, 1975; Owen et al. 1990).

The *Solvik Formation* consists mostly of dark shale with alternating thin layers of siltstone and limestone. The lower boundary is easily differentiated from the Langøyene Formation with the abrupt change from sandstone to shale. Nodules of limestone may also be visible at the base of the formation. The thickness is estimated to approximately 190 m (Baarli, 1985).

The *Rytteråker Formation* is limestone dominated with an estimated thickness of 50 m. The lower boundary is made up of interbedded thin to medium siltstones and shales alternating limestone beds. The thickness of limestone and calcareous shale differs throughout the formation. Planar limestone beds and bedded calcareous nodules with interbedded shales make up the upper boundary, with an increase of shale content towards the overlying Vik Formation (Worsley et al. 1983).

The *Vik Formation* is estimated to a thickness of 80 m, with varying parts of red and greenish grey shales and limestone. The contact between the underlying Rytteråker Formation is defined as a sharp transition from limestone to a more shale dominated unit. Thin bedded limestone nodules and continuous limestone make up the middle part of the Vik Formation. The Upper boundary of the Vik Formation is made up of greenish grey shales (Worsley et al. 1983).

The *Skinnerbukta Formation* consists of dark grey graptoliferous shales, with occasional thin calcareous rich zones. Towards the upper boundary of the formation, the calcareous content increases and the uppermost parts are made up of paler calcareous shales. This formation is also estimated to a thickness of approximately 80 m (Worsley et al. 1983).

The contact to the *Malmøya Formation* is recognized by continuous limestone beds overlying the graptoliferous shales of the Skinnerbukta Formation. Varying sections of continuous, nodular and lensoid limestone beds with interbedded shales make up the lower parts of the

formation. Towards the top of the formation thick to massive bedded biosparitic limestones occur. The formation is estimated to a thickness of 35 m and is the youngest preserved strata of Silurian age in the Oslo area (Worsley et al. 1983).

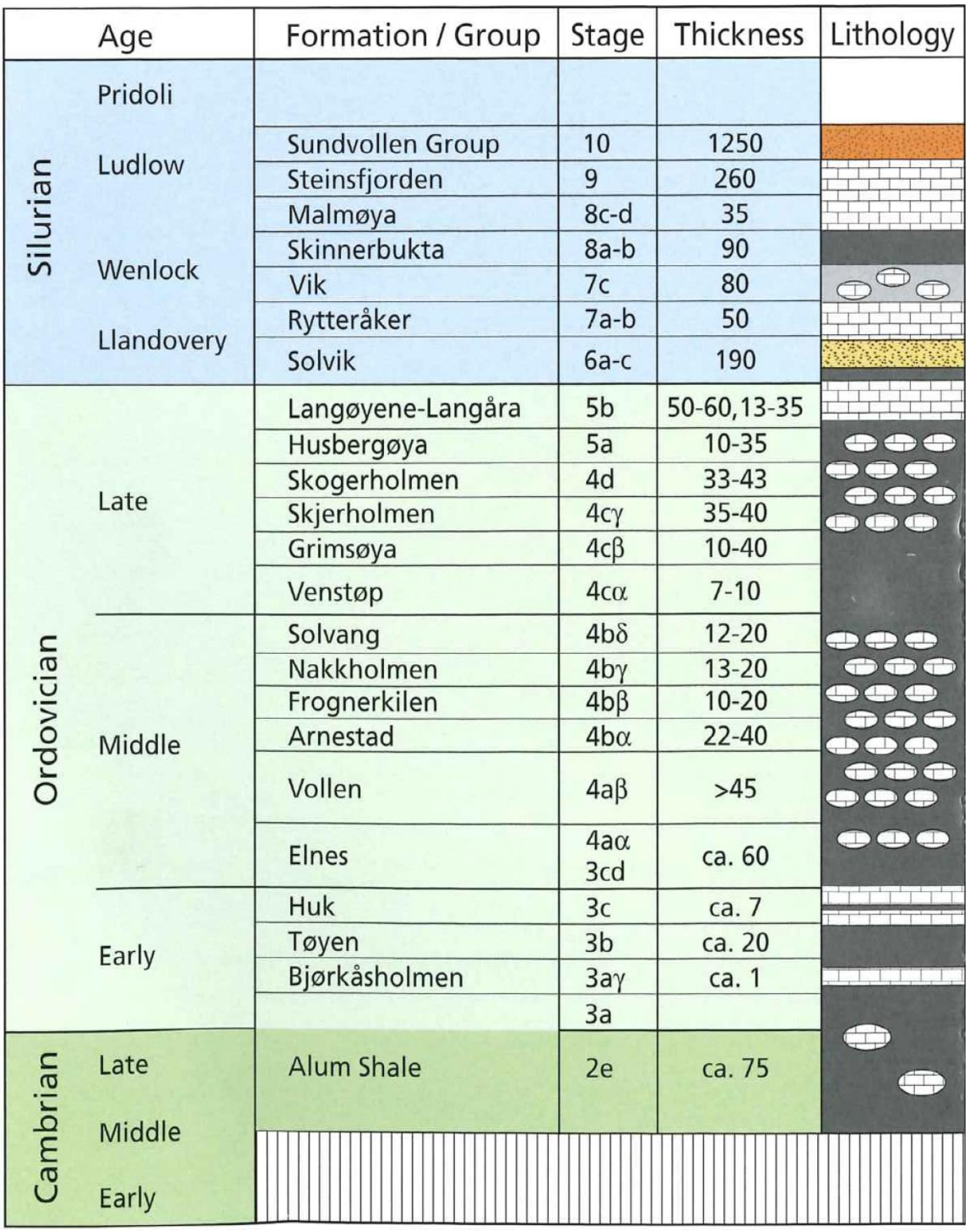

Age		Formation / Group	Stage	Thickness
Silurian	Pridoli			
	Ludlow	Sundvollen Group	10	1250
		Steinsfjorden	9	260
		Malmøya	8c-d	35
	Wenlock	Skinnerbukta	8a-b	90
		Vik	7c	80
	Llandovery	Rytteråker	7a-b	50
		Solvik	6a-c	190
Ordovician	Late	Langøyene-Langåra	5b	50-60,13-35
		Husbergøya	5a	10-35
		Skogerholmen	4d	33-43
		Skjerholmen	4cγ	35-40
		Grimsøya	4cβ	10-40
		Venstøp	4cα	7-10
	Middle	Solvang	4bδ	12-20
		Nakkholmen	4bγ	13-20
		Frognerkilen	4bβ	10-20
		Arnestad	4bα	22-40
		Vollen	4aβ	>45
		Elnes	4aα 3cd	ca. 60
	Early	Huk	3c	ca. 7
		Tøyen	3b	ca. 20
		Bjørkåsholmen	3aγ	ca. 1
			3a	
Cambrian	Late	Alum Shale	2e	ca. 75
	Middle			
	Early			

Figure 5.1: Thickness in meters of stratigraphy from the study area. Figure modified from Nakrem and Worsley (2008). Sundvollen Group corresponds to Ringerike Group

5.2 Extension

5.2.1 Intrusions

Four general types of intrusions are mapped from the study area, including lamprophyres, rhomb porphyry, diabase and syenite porphyry, mainly as dikes cutting the bedding almost perpendicular in a dominantly NNW-NNE direction (appendix A). A few intrusions appearing as sills were also mapped.

The lamprophyres were only found two places within in the study area. One on the farwest side of Rambergøya where it occurs as a sill and the other one dike on the east side of Malmøya, close to the beach (appendix A). They have a yellow-brownish to black/grey color on the weathered surface and a darker color in fresh surface, and they are approximately 130 cm wide. Small looking bumps on exposed surface was observed, these represents ocelli. On Rambergøy the lamprophyre sill had a W-E direction (044/63) perpendicular to most of the intrusives in the area (fig 5.2). On Malmøya the dike more or less follows the same trend (140/55) as the surrounding dikes.

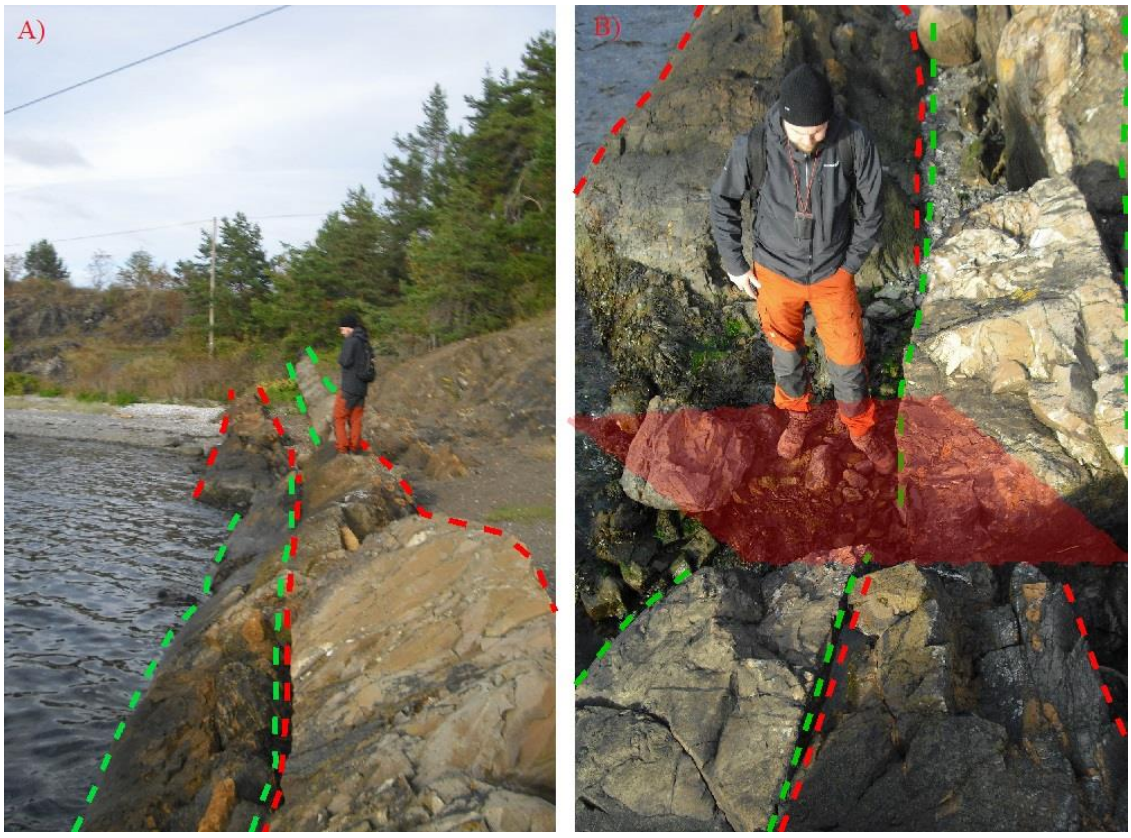

Figure 5.2: Picture A) shows the lamprophyre found on Gressholmen marked with the red dotted line running parallel with the syenite marked with green dotted line. In picture B) one can see the lamprophyre cutting the parallel syenite marked.

The two thin sections from Rambergøya and Malmøya (fig 5.3) both contain ocelli which are common to find in some lamprophyres. The dominant mineral content of both samples was; amphibole, feldspar, oxides, chlorite, biotite, calcite, apatite and carbonates. There was no big notable difference between the two samples in mineral content.

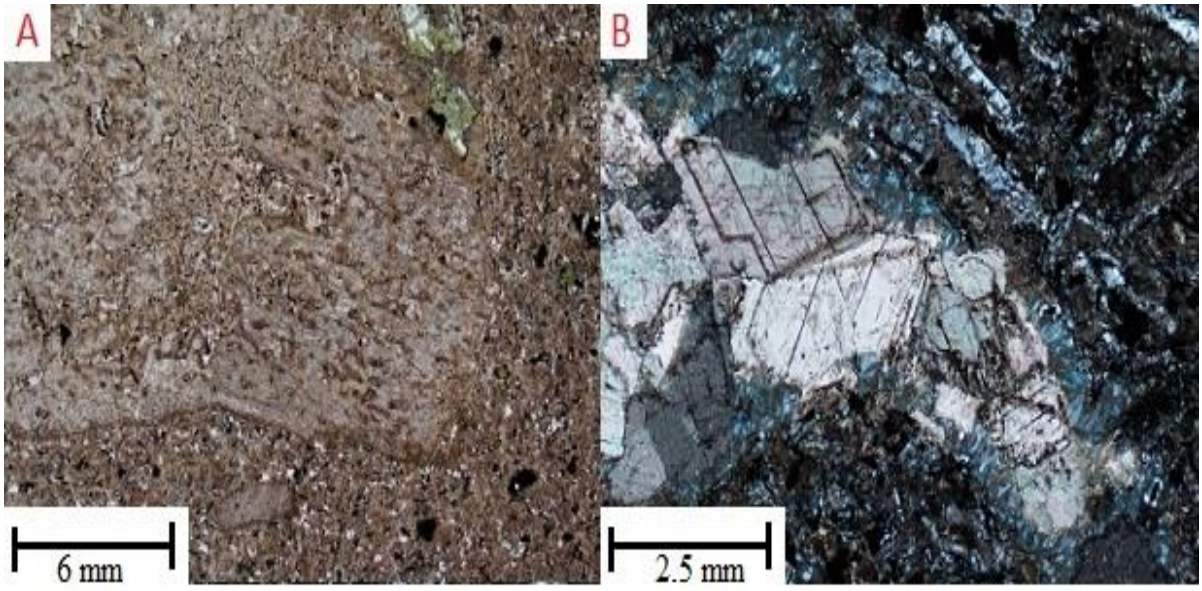

Figure 5.3: Thin sections from the two lamprophyres. A) Displays the lamprophyre found at Gressholmen in plane polarized light, while B) shows the lamprophyre found at Malmøya in crossed polarized light. The large calcite and alkali feldspar crystals from ocellis in the groundmass in both lamprophyres.

The rhomb porphyry dikes are the biggest/widest dikes found in the study area varying between 10-15 m in thickness. Weathered surfaces have a reddish color while fresh surfaces show a variation of grey from dark to semi dark. Well-developed pale rhombic phenocrysts, with various size from less than 1 cm up to approximately 4 cm, are found within a finer darker grained matrix (fig 5.4). One rhomb porphyry with its distinct characteristics can be followed all the way from Husbergøya through Langøyene and Gressholmen, on the western sides of the islands. From Gressholmen it makes a 90° turn passing through Lindøya (W-E), parallel with the bedding. Finally, it reaches the western center of Hovedøya before making a new 90° turn, lying perpendicular to the bedding again in the direction of Akershus Festning. A second large rhomb porphyry dike observed at the western most part of Nakkholmen, that follows the length of the island is interpreted to be connected with a rhomb porphyry at Huk based on previous maps by W.C Brøgger (1885). No other dikes in the area has been possible to follow over such a long distance.

Figure 5.4: Rhomb porphyry with the well developed rhombic phenocrysts from A) Husbergøya and B) Langøyene. Field book as scale.

The syenite dikes show the biggest variation in width, ranging from ca. 1 m up to almost 10m. In weathered surface they vary from brownish-yellow to greenish-grey and in fresh surface they display a pinkish to grey color (fig 5.5). The syenite dikes appear to be coarser grained than the rhomb porphyry and diabase intrusions. White feldspar phenocrysts are found within the matrix along with green minerals interpreted as chlorite. The syenite phenocrysts are considerably smaller than the phenocrysts found in the rhomb porphyry, with a maximum observed size of less than 1 cm. At Lindøya and Gressholmen syenite porphyry also appeared as sills.

Figure 5.5: Two syenite dikes, both part of a composite dike complex followed from A) Hovedøya over to B) Bleikøya.Field book as scale.

The two thin sections in (fig 5.6) was sampled from Hovedøya and Bleikøya respectively (fig 5.5). The dominating mineral in both samples was the altered feldspar which was seen as elongated phenocrysts in the field. Other minerals found in the thin sections were; amphibole, pyroxene and chlorite, formed as an alteration product, in varying amount.

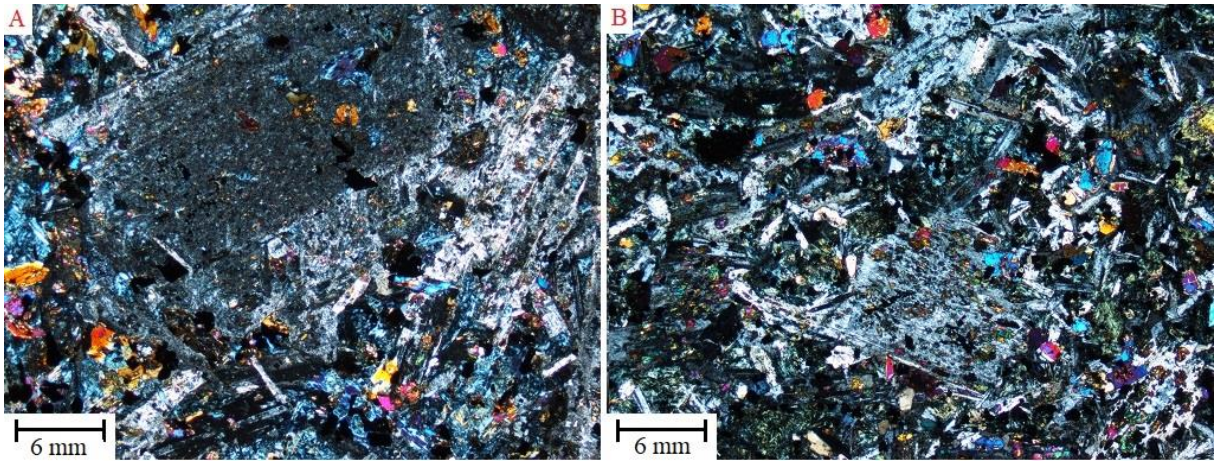

Figure 5.6: Thin sections from the syenite on A) Hovedøya and B) Bleikøya, both in crossed polarized light.

The dominant type of intrusions found in the study area are the diabase dikes (fig 5.7). They are found multiple places on all mapped locations, ranging in size from approximately 20 cm up to about 6 m. In weathered surface they display a reddish to brown color, while in fresh surface they are grey. Phenocrysts are also visible in most of the diabase dikes where they tend to be collected in the center of the dikes, with an average size of 3 mm. The surrounding matrix is fine grained with evidence of gas bubbles.

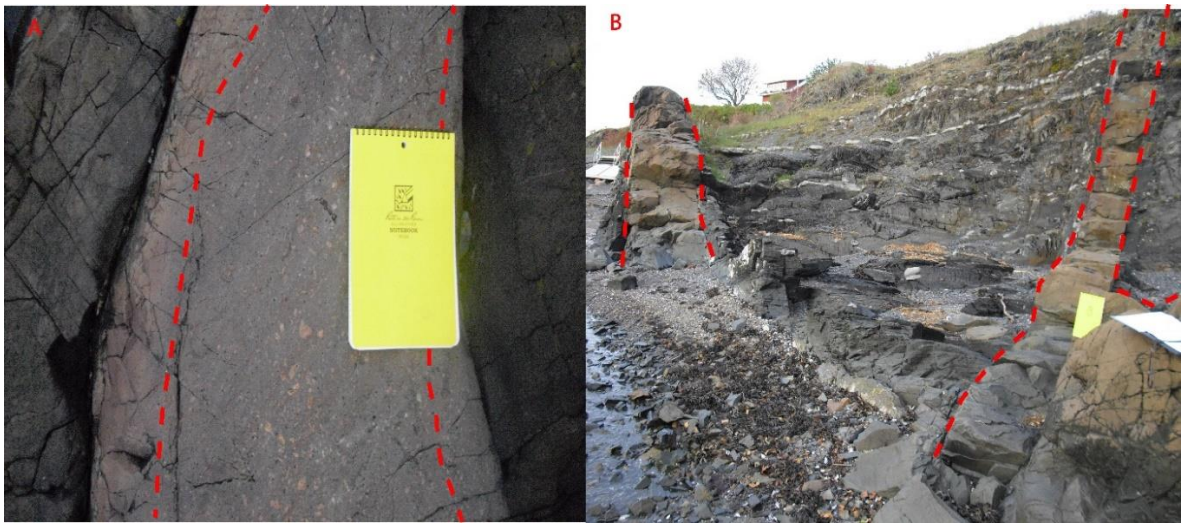

Figure 5.7: Two diabase intrusions from A) Gressholmen and B) Nakkholmen. In picture A) it is possible to see the collection of phenocrysts towards the middle of the dike. While picture B) displays the variation in size of the diabase intrusions and orientation. Field book as scale.

5.2.2 Orientation of intrusions

As stated above the majority of the dikes are oriented NNW-SSE, while the few sills that were mapped show a bedding parallel orientation in an NE-SW direction (fig 5.13).

The diabase and rhomb porphyry dikes show the most consistency in orientation with little to none divergence from the main NNW-SSE orientation when plotted in a stereonet. Only the measured rhomb porphyry at Lindøya with a W-E orientation after the 90° turn stands out from the rest (fig 5.12 and fig 5.10).

The syenite dikes and sills show three major orientations when plotted in a stereonet. An NNW-SSE, N-S and NE-SW direction. The syenite sills on Lindøya are interpreted to make a 90° turn coming from Gressholmen, just like the rhomb porphyry (fig 5.9 and fig 5.11).

Based on the stereographic projections of the different types of dikes mapped within the study area dip it is clear that the dip varies between 70° to being vertical. A common factor is that the dikes being sub-vertical often are associated with normal faults.

In some places especially around Hovedøya the diabase dikes show a tendency to "jump" (fig 5.8).

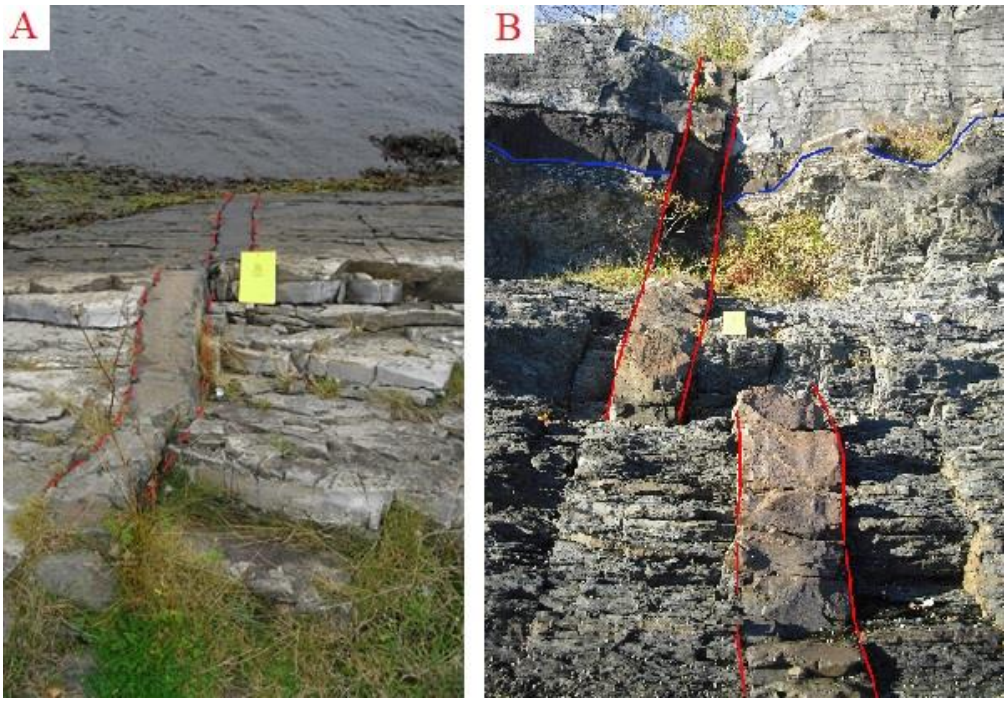

Figure 5.8: Two diabase dikes on Hovedøya, A) and B) which has performed a "jump, marked with red lines. In picture B) the blue line represents the Ordovician to Silurian boundary. No offset was recorded together with either dike. Field book as scale.

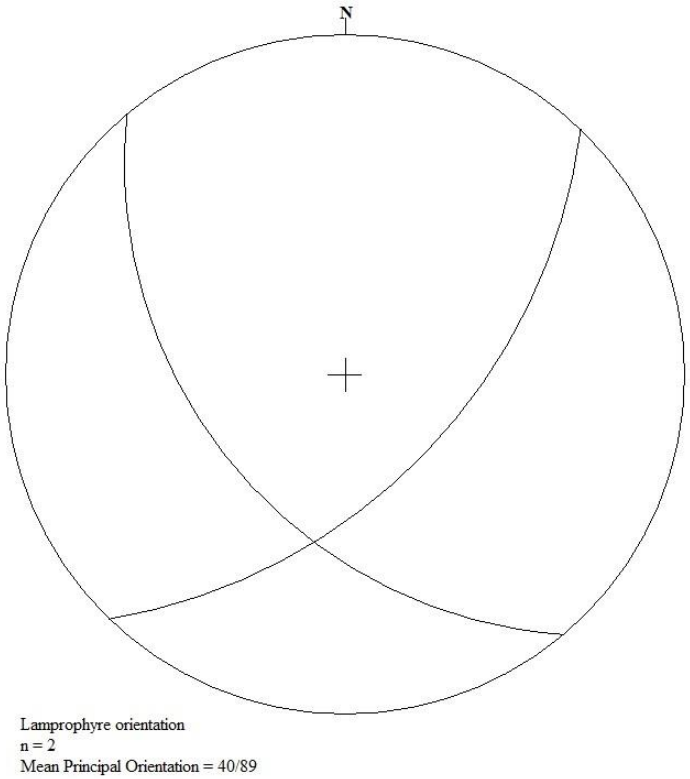

Figure 5.9: Stereographic projection of the mapped Lamprophyre sill and dike on Rambergøya and Malmøya respectively.

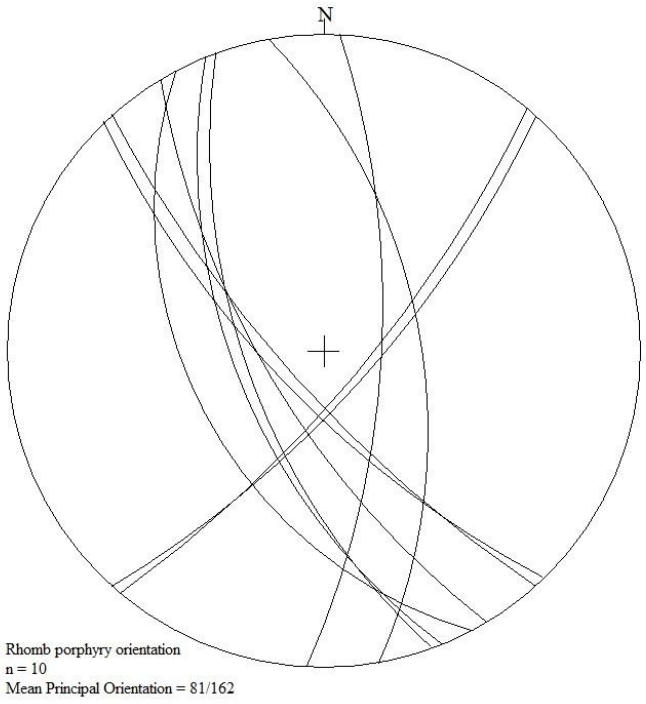

Figure 5.10: Stereographic projection of the mapped rhomb porphyry dikes within the study area.

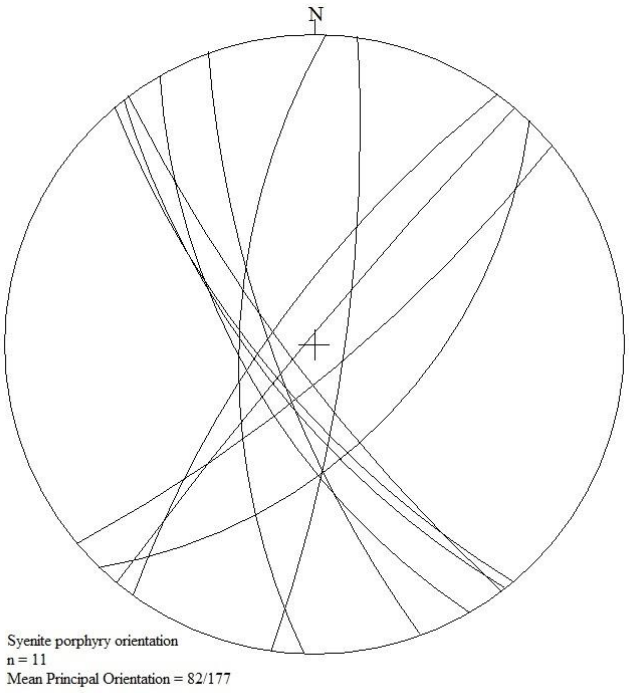

Figure 5.11: Stereographic projections of the mapped syenite porphyry dikes and sills within the study area.

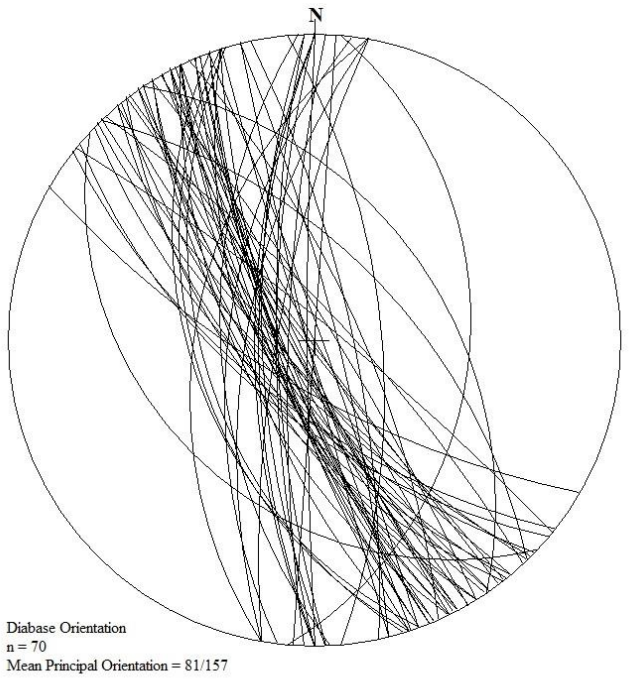

Figure 5.12: Stereographic projections of the mapped diabase dikes within the study area.

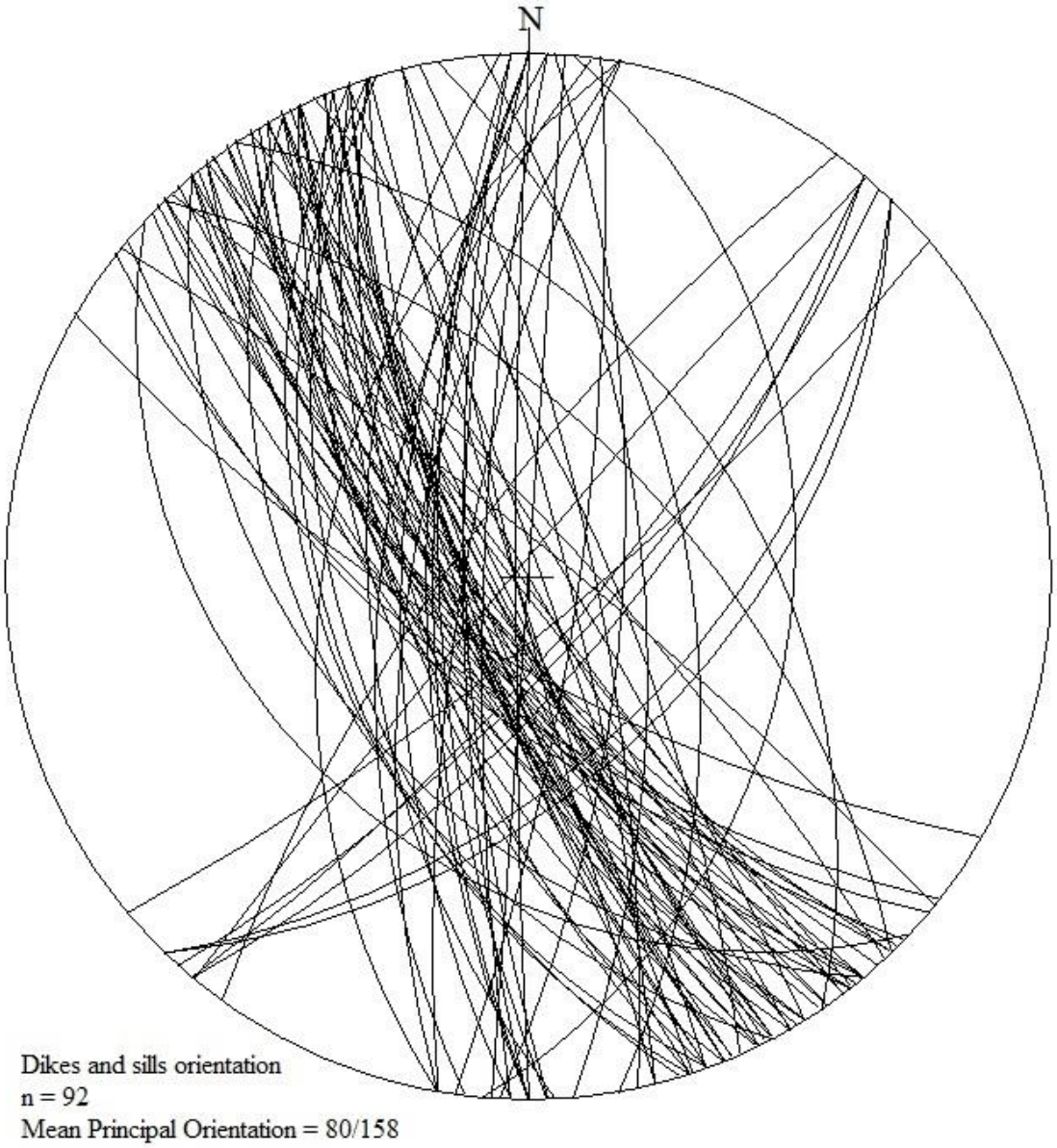

Figure 5.13: Stereographic projections of all mapped sills and dikes within the study area.

Like the rhomb porphyry which has been interpreted to be followed from Husbergøya to Hovedøya crossing several islands, other intrusions show the same sign. These interpretations are based on strike, width and appearance of the dikes recorded in the study area and previous work by Brøgger (1885). The interpreted dikes crossing between islands are mapped in appendix A.

5.2.3 Calculation of extension

All the NNW-SSE and N-S trending dikes have been used in the calculation of extension within the study area (appendix A). This was done by drawing W-E transects across the study area in two places. One from Nakkholmen across Lindøya and Hovedøya in the direction of Ekerberg and another one from Gressholmen across to Bleikøya. The width of each dikes within each transect was added to get the total amount of extension in the W-E direction interpreted with the dikes extrapolated. Absolute thickness was used, as the dikes more or less are subvertical. The result of the calculation is seen in table 5.1 and 5.2.

Table 5.1: The total amount of extension based on the width of the dikes mapped within the study area on each island and in total, in a W-E transect from Nakkholmen to Hovedøya (3000 m).

ISLANDS	NUMBER OF DIKES	AMOUNT OF EXTENSION (m)	AMOUNT OF EXTENSION per Km
Nakkholmen	6	29,74 m	
Lindøya	13	22,37 m	
Hovedøya	20	48,01 m	
TOTAL		**100,12 m**	**30 m/Km**

Table 5.2: The total amount of extension based on the width of the dikes mapped within the study area on each island and in total, in a W-E transect from Gressholem to Bleikøya (2682 m).

ISLANDS	NUMBER OF DIKES	AMOUNT OF EXTENSION (m)	AMOUNT OF EXTENSION per Km
Gressholmen	17	57,01 m	
Bleikøya	11	28,37 m	
TOTAL		**85,38 m**	**31 m/Km**

The difference in total amount of extension differs little between the two transects. When calculated into meters of extension per kilometres the transect from Nakkholmen to Hovedøya results in 30 m/km and for the transect between Gressholmen and Bleikøya the extension is 31 m/km. This gives a relative stretching factor of only 3% and a β-factor of 1.03 within the fault block of the study area, when only the dikes are taken in account.

5.3 Displacement across faults and intrusions

5.3.1 Orientation of normal faults

The mapped normal faults within the study area show an NNW-SSE and N-S principal orientation with an average dip of 65°. From stereographic projections the calculated mean principal orientation of the mapped normal faults is 159/89, strike and dip respectively (fig 5.14).

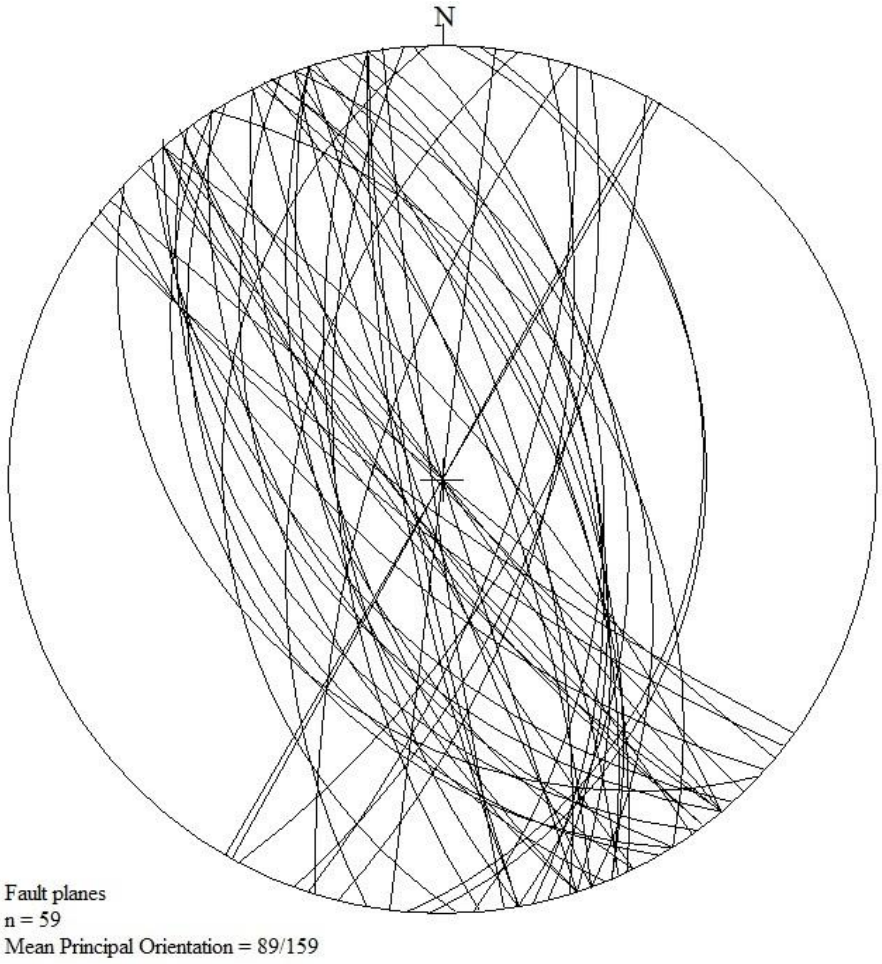

Figure 5.14: Stereographic projection of all the normal faults within the study area.

Throughout the area normal faults display a variety of different dips. The largest faults, regarding offset, often associated with dikes (appendix A) are near subvertical. Lineations found in association with the fault planes in calcite is typically also subvertical. The presence of minor faults, both antithetic and synthetic are on most islands found increasing in density

closer to the larger folds. The minor antithetic and synthetic secondary faults are found on almost every island with a displacement varying from only a couple centimetres to almost a meter. They usually show a gentler dip compared to the dike related faults, but they may also occur as subvertical faults (fig 5.16 and 5.17).

5.3.2 Observed normal faults

On Hovedøya a normal fault on the southwest side of the island shows a clear displacement between the layers of Ordovician and Silurian age across the fault (fig 5.15). In conjunction with the normal fault an intrusive diabase has forced itself up in the weakened zone. The displacement across the fault has been measured to approximately 7 m in field, with an orientation of strike and dip equal to 140°/82°. The bedding on both sides of the fault is overturned being on the overturned limb of the Hovedøya anticline. There is little to no variation in dip and strike on the two sides of the fault.

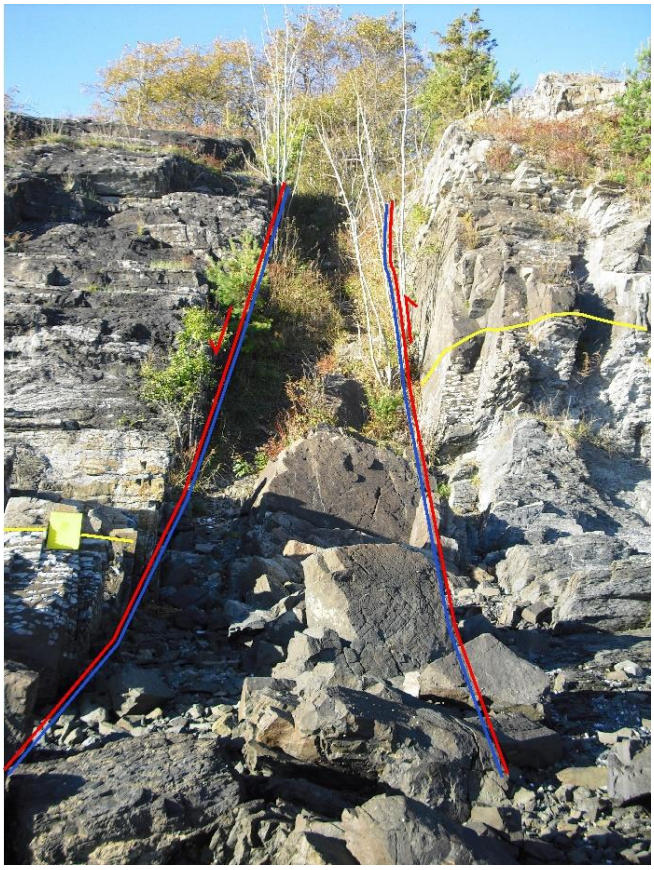

Figure 5.15: The picture displays a normal fault with displacement of approximately 7 meters, faulting the Ordovician and Silurian boundaries marked by the red lines. The blue line markes the intrusive dike following the same orientation as the fault itself. The yellow line represents the the Ordovician to Silurian boundary.

Figure 5.16: Two minor normal faults recorded at A) Nakkholmen and B) Gressholmen, Stereographic projection of the two fault planes can be seen in figure 5.17.

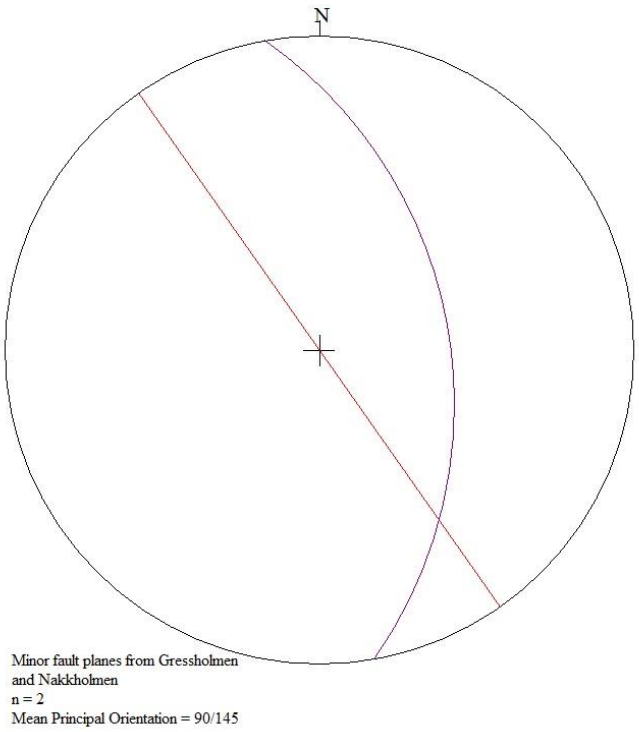

Figure 5.17: Stereographic projection of the two minor faults recorded from figure 5.16 at Gressholmen (red line) and Nakkholmen (purple line). The recorded orientation was; Gressholmen (145/90) and Nakkholmen (350/56)

The minor faults recorded within the study area, such as the ones in (fig 5.16) never display an offset of more than 60 cm. Most commonly the observed displacement is just a couple of centimetres.

On Gressholmen the core of the Gressholmen anticline consisting of limestone interbedded with calcareous shale is exposed on the western most part of Rambergøya. At the base of the anticline core there is a visible normal fault with a N-S orientation with a dip 86° to the west and lineation oriented 056°/87°. A specific sequence of alternating limestone and shale interpreted as the Vollen Formation after Owen et al. (1990) at the base of the anticline was used as reference layer suggesting a displacement of 7,5 meters (fig 5.18).

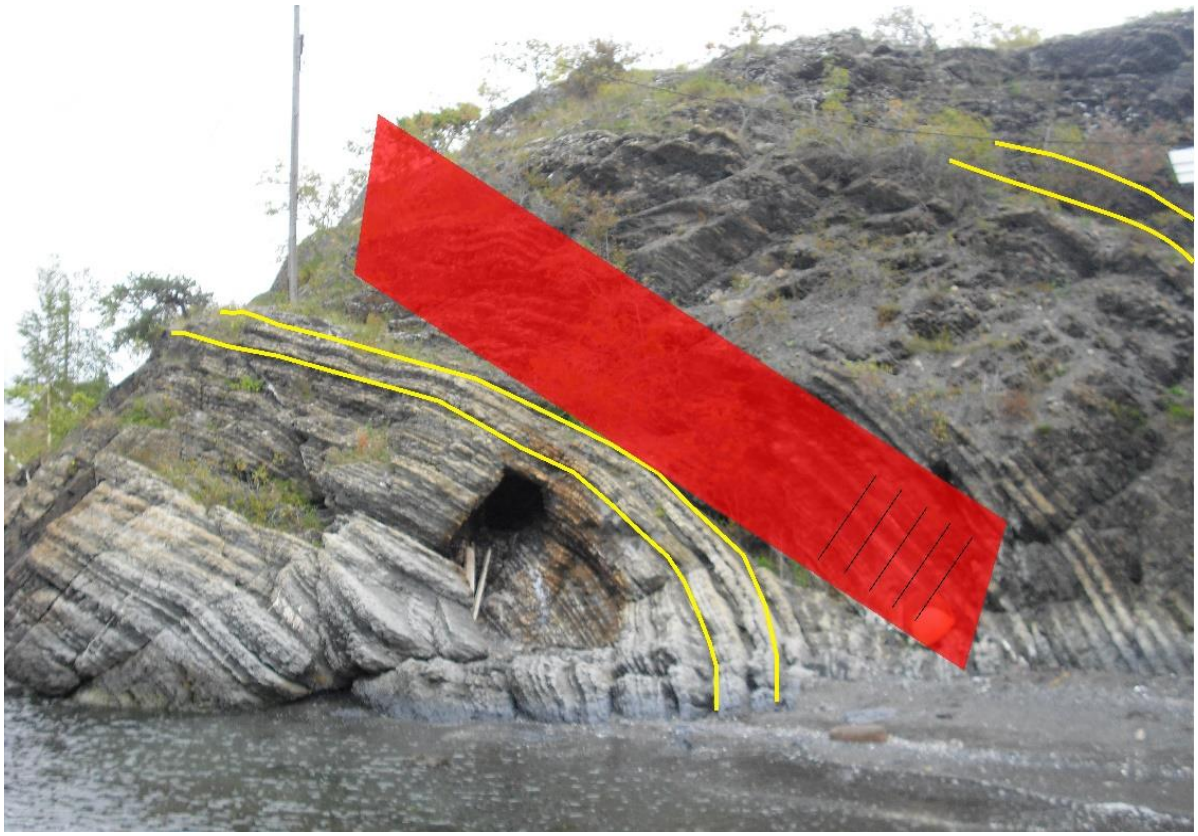

Figure 5.18: The core of the Gressholmen anticline. The fault marked with the red rectangle with a strike-dip orientation of 180/87. The black lines within the rectangle represents the lineation with a recorded orientation of 56°. The displaced reference layer is marked with a yellow line. Orientation of dip fault plane is 87° and the displacement was measured to 7,5 m in field.

A W-E profile perpendicular to the normal faults from across Gressholmen and Bleikøya is shown in (fig 5.19 and (appendix H). The main fault has been interpreted to lie between the two islands with a calculated maximum displacement of 102 meters (appendix A), based on the calculation method described in chapter 3. The method where the fold axis on one of the islands is not reconstructed because of a "missing fold limb. The displacement along the faults on both sides of the main fault vary from 3 meters up to 52 meters, with the most offset along a diabase dike on Bleikøya (appendix A). Other faults may be present in the cross-section but are not visible on the surface. The thickness of the layers has been extrapolated across to Bleikøya along with the β-axis of 13° as only one of the fault limbs are visible at Bleikøya.

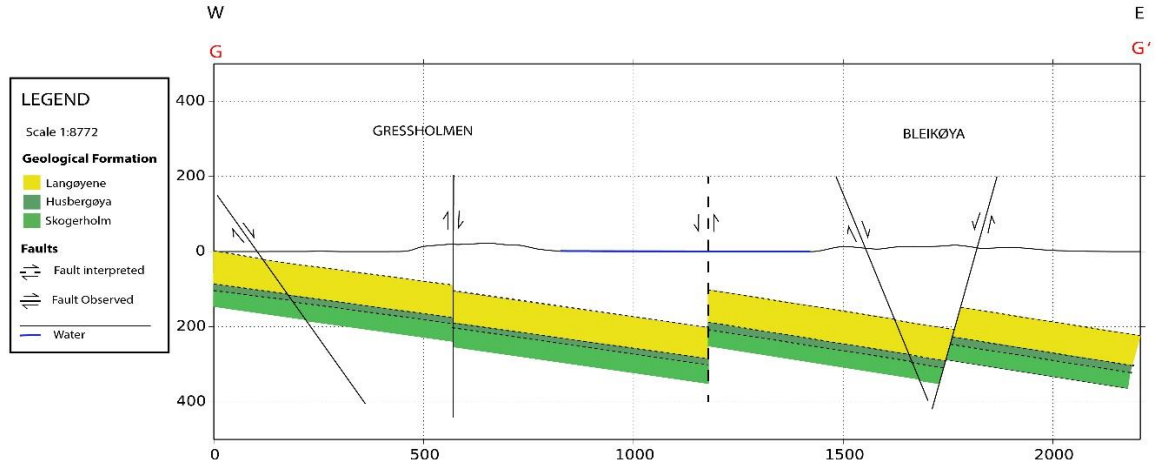

Figure 5.19: W-E cross section from Gressholmen across to Bleikøya displaying the major faults and their displacement.

5.3.3 Displacement calculations

Following the different methods described in chapter 3, the amount of displacement on each island has been calculated along with the displacement across three W-E transect from Lindøya to Hovedøya, Gressholmen to Bleikøya and from Malmøya to Ulvøya. The results from the calculations can be seen in table 5.3 and 5.4.

Table 5.3: The table displays the number of larger faults and the total vertical displacement in meters observed on each island within the study area.

ISLANDS	NUMBER OF FAULTS	VERTICAL DISPLACEMENT (m)
Hovedøya	6	71
Gressholmen	3	94
Bleikøya	2	58
Husbergøya	2	21
TOTAL	**13**	**244**

Table 5.4: The calculated displacement over each W-E segment within the study area.

W-E SEGMENT	TOTAL VERTICAL DISPLACEMENT (m)	TOTAL VERTICAL DISPLACEMENT (m/Km)
Lindøya -> Hovedøya	71	5
Gressholmen -> Bleikøya	102	4
Malmøya -> Ulvøya	190	2
TOTAL	**363**	**11**

The total vertical displacement in the W-E segment, vary only 3 m/Km. In the north of the study area the neighbouring W-E segments of Lindøy-Hovedøya and Gressholmen-Bleikøya only vary with 1 m/Km. The reason for bigger displacement between Malmøya and Ulvøya might be the close vicinity of the Ekeberg Fault.

5.4 Folds

Introduction

The recording of Caledonian structures such as folds are not a part of this thesis, but profiles based on previous work by Dehli (2012) and Repshus (2012) along with data recorded data through this thesis have been used to create cross section profiles for the use of estimating displacement and interpretation of fault block rotation.

5.5 Fold axis and fold geometry

The study area consists of a series of anticlines and synclines formed as a fold train, with Nakkholmen being the only visible syncline above sea level. The folded bedding is interpreted to have formed by compression during the structural development of the Scandinavian Caledonides.

The folds throughout a segment of the study area (fig 5.20 and appendix G) show near uniform fold axis orientation only varying between 6° and 14°, with Ulvøya at 0° closest to the Ekeberg fault. The fold axis shows an increase in plunge southward and westward from the Ekeberg fault. The cross-section created in figure 5.20 shows that the wavelength and amplitude of the folded islands more or less stay the same throughout the study area. At the very most SSE section there is a discontinuity in fold geometry, with Nordre and Søndre Skjærholmen deviating from the fold pattern. It has been interpreted that a reverse fault is the cause of this repeated limb. It is also clear from the profile that the amount of overturning decreases southwards in the study area.

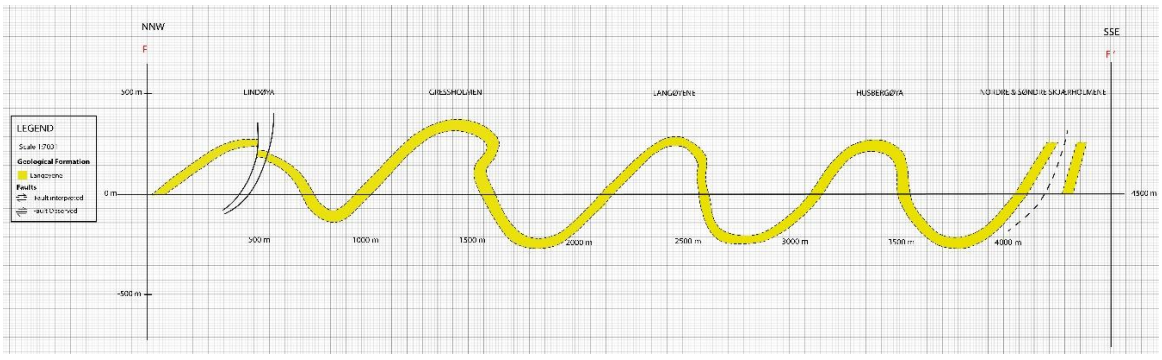

Figure 5.20: Cross-section of the study area in a NNW-SSE direction. The folds show little to none variation in wavelength and amplitude. However, in SSE corner a reverse fault has been interpreted as the wavelength suddenly changes and the two islands of Nordre and Søndre Skjærholmen display the same dip orientation on the exposed fold limb.

Parasitic folds are found throughout the study area replicating the orientation of the main folds of the different islands (fig 5.21).

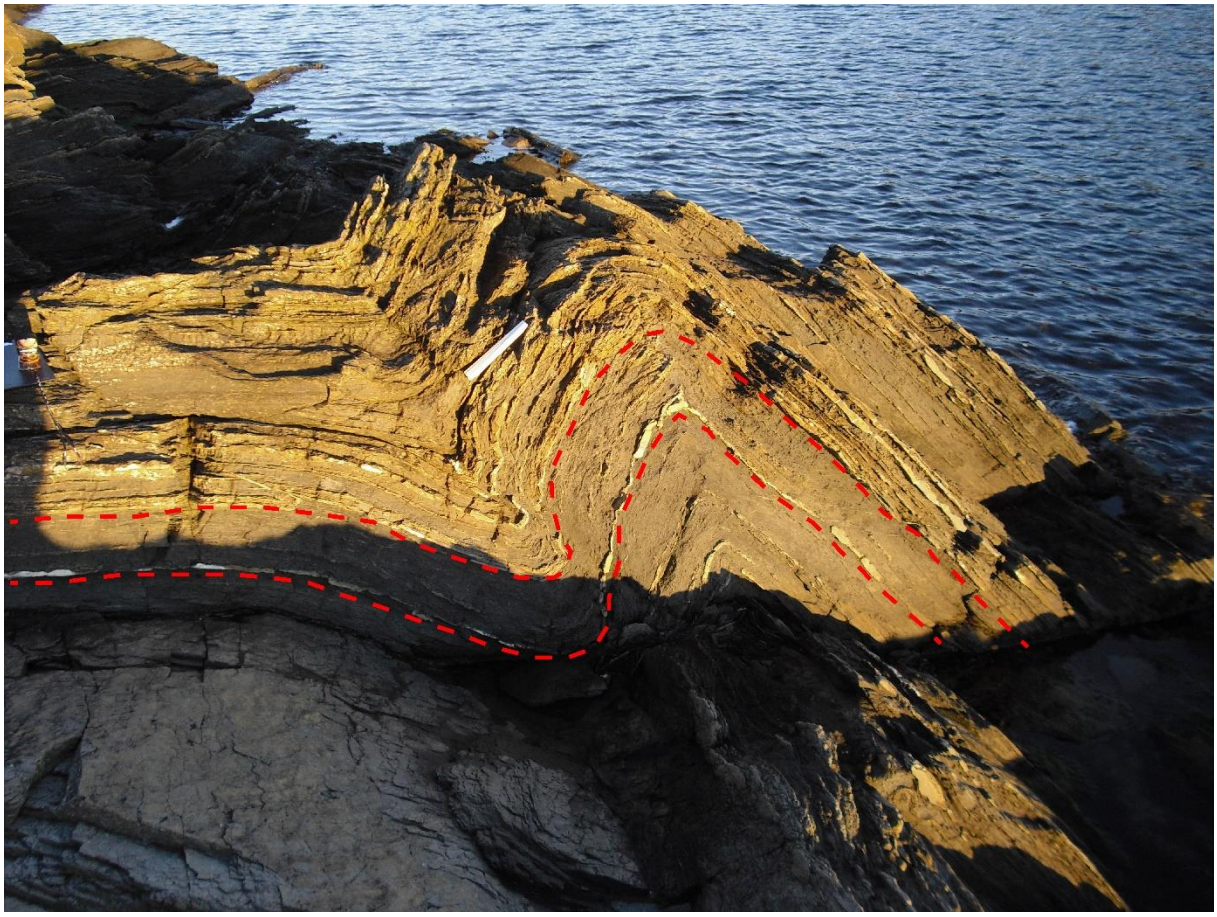

Figure 5.21: Parasitic fold found on Malmøyakalven, reflecting the orientation of the southern most fold of the neighbouring island Malmøya.

5.6 Stereographic projection for estimations of fold geometry

When plotting the bedding of the different islands for stereographic projections (fig 5.22 and fig 5.23), two separate plots were made to qualify that the fold axis and the calculated axial plane was correct due to the overturned limbs on some of the islands. This was done by first plotting all of the bedding measurements in one stereonet and afterwards quality checking by taking the central point of the contours of each limb. This resulted only in minor difference on the fold axis and axial trace, therefor all the stereographic projections are made from all measured bedding except Nakkholmen. In the case of Nakkholmen the contours were used to find the axial trace (fig 5.23A and fig 5.24).

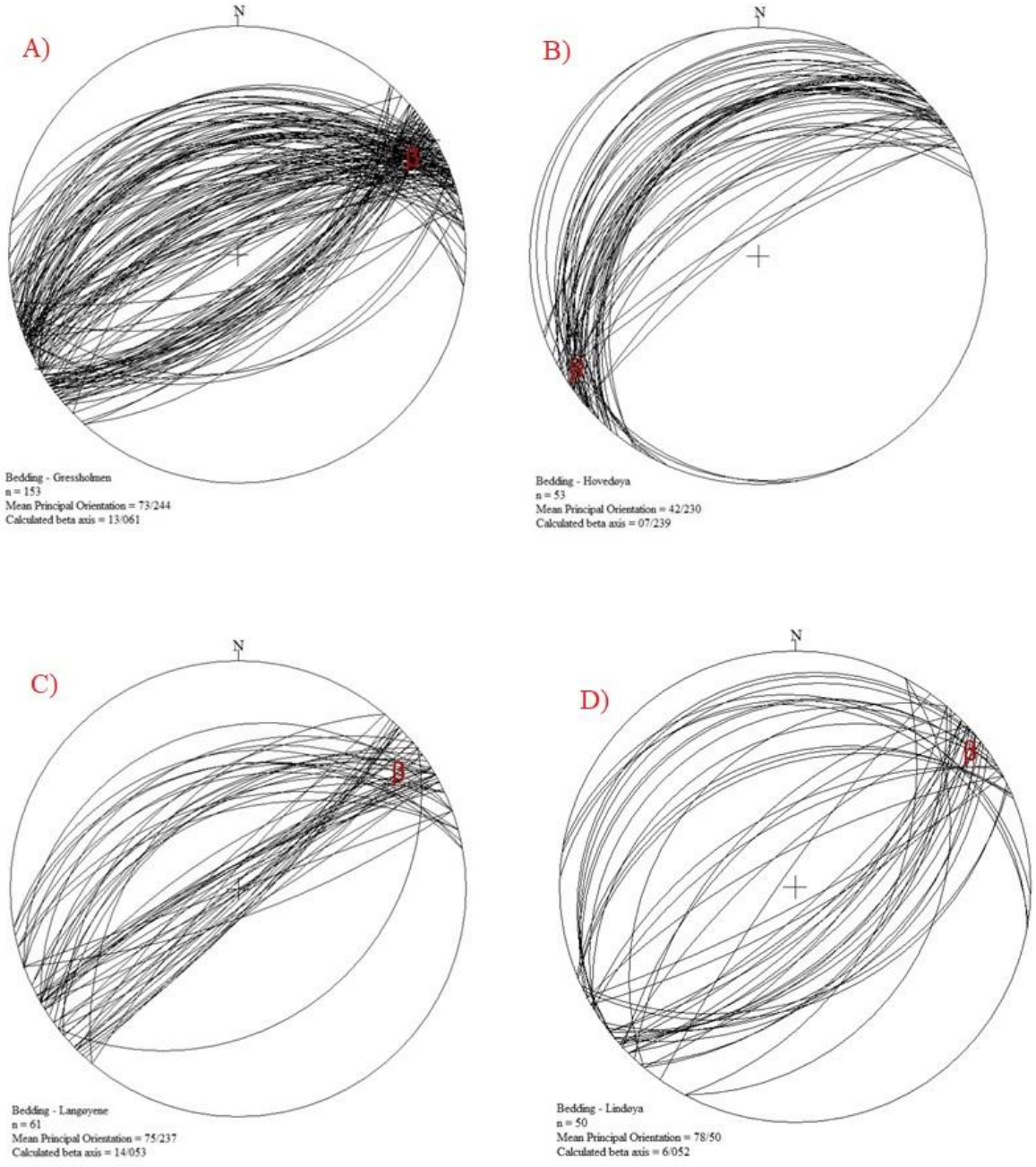

Figure 5.22: Stereographic projections of bedding for the calculation of fold axis (β) and axial plane for the islands; A) Gressholmen, B) Hovedøya, C) Langøyene and D) Lindøya.

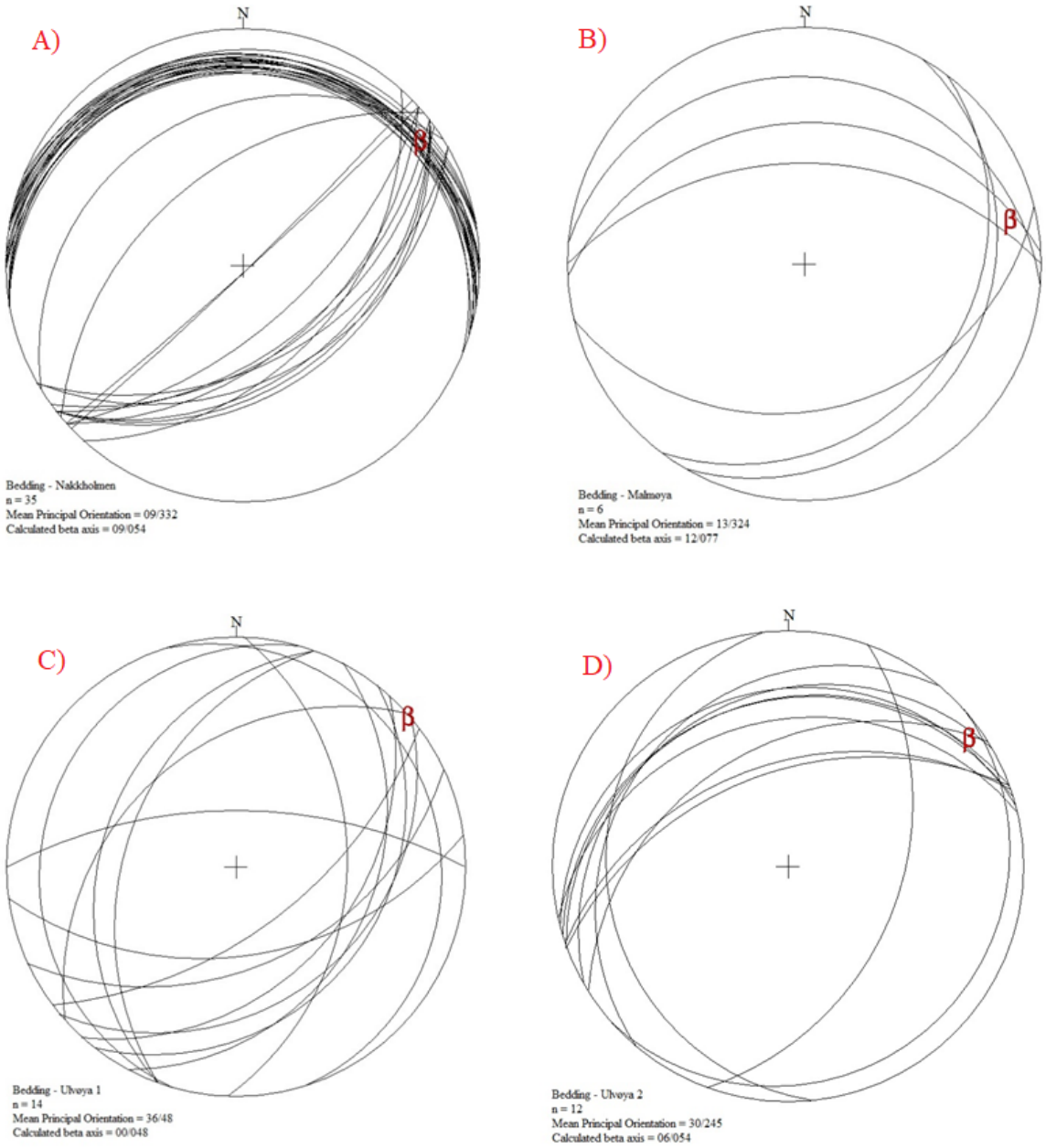

Figure 5.23: Stereographic projections of bedding for the calculation of fold axis (β) and axial plane for the islands; A) Nakkholmen, B) Malmøya C) Ulvøya anticline and D) Ulvøya syncline.

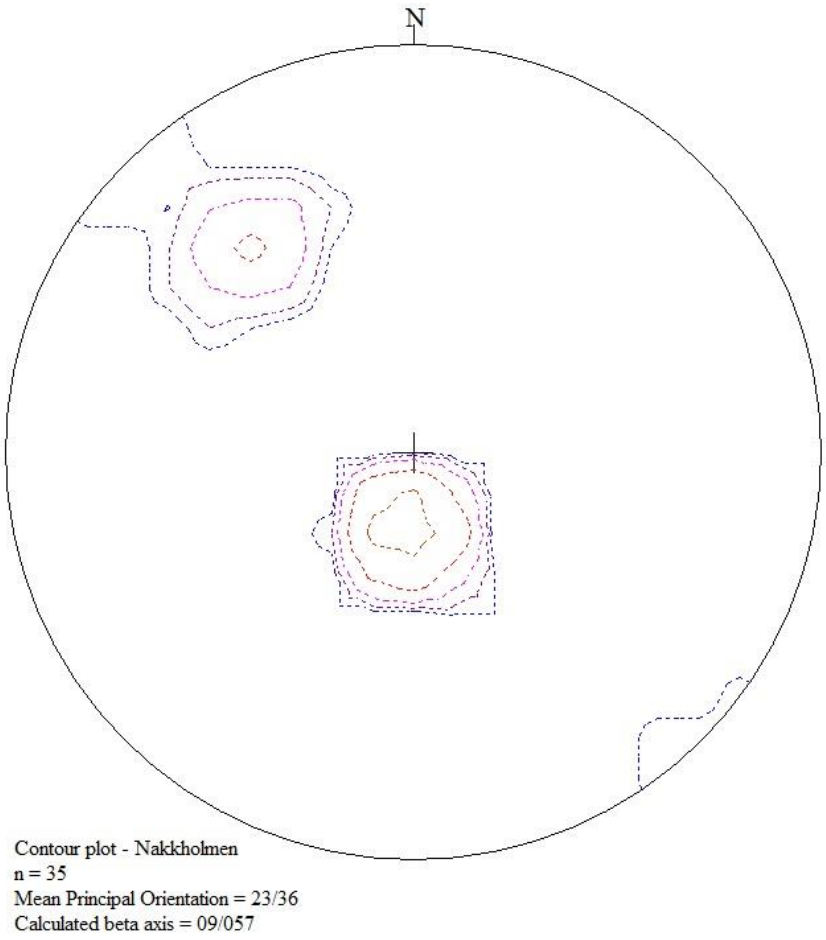

Figure 5.24: Contour plot of the Nakkholmen bedding made to quality check Stereographic projections of the axial planes of the folds.

The calculated axial plane from bedding measurements within the study area together with field observations of the fold geometry were used to reproduce the fold geometry of the different islands in the following profiles (fig 5.26, 5.27, 5.28, 5.29 and 5.30).

Based on bathymetry data from GEONORGE (fig 5.25) it is possible to interpret the eroded fold limb of bleikøya and it also seems that the fault geometry in the NNW-SSE direction of the study area is restored after Søndre Skjærholmen (appendix A).

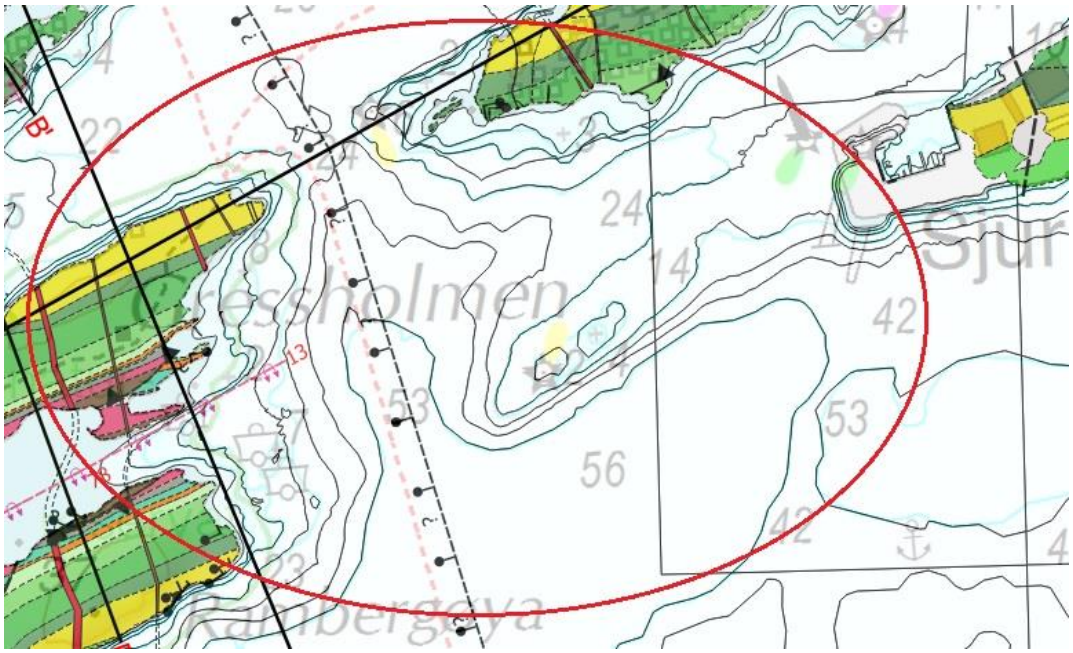

Figure 5.25: Detail from appendix A, with the red circle indicating the eroded fold limb of Bleikøya interpreted from bathymetry data.

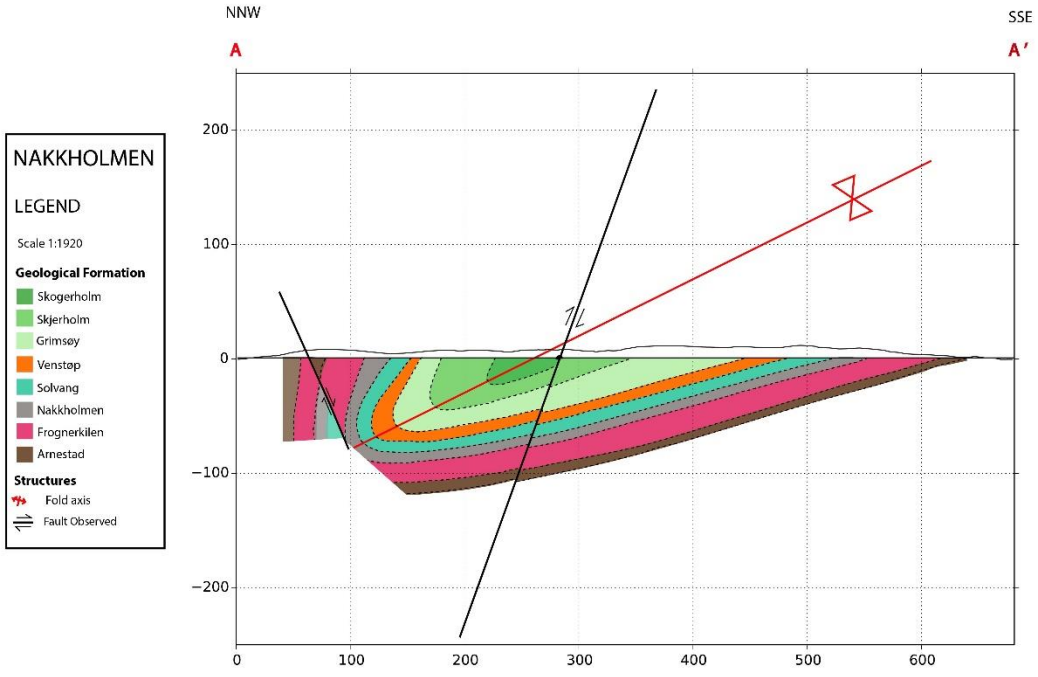

Figure 5.26: Cross section profile of Nakkholmen (for profile in A3 size, see appendix B)

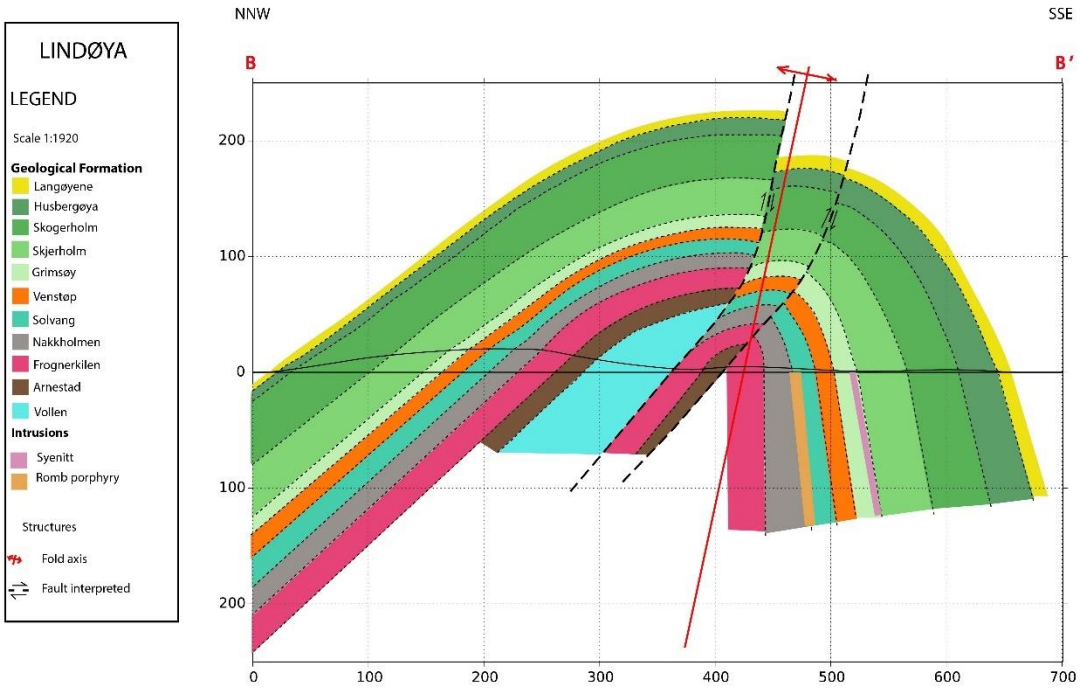

Figure 5.27: Cross section profile of Lindøya (for profile in A3 size, see appendix C)

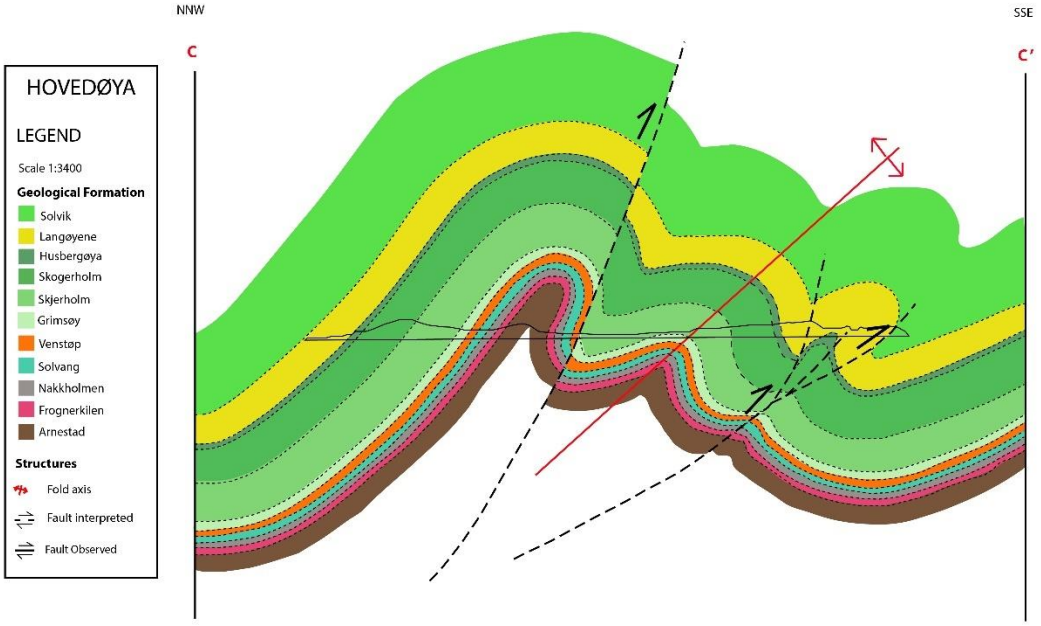

Figure 5.28: Cross section profile of Hovedøya, modified from Repshus (2012). For profile in A3 size see appendix D.

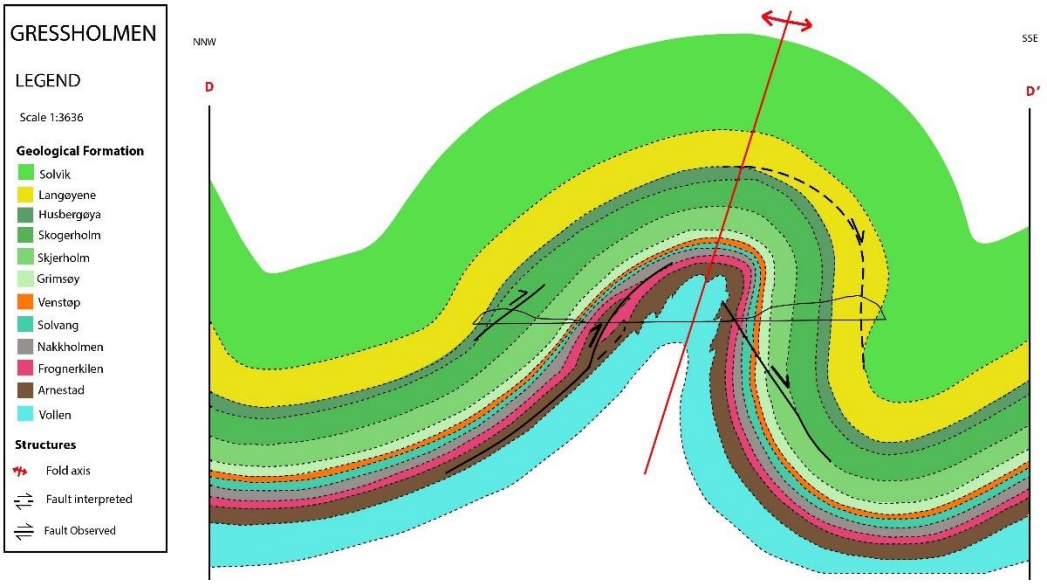

Figure 5.29: Cross section profile of Gressholmen, modified from Dehli (2012). For profile in A3 size, see appendix E.

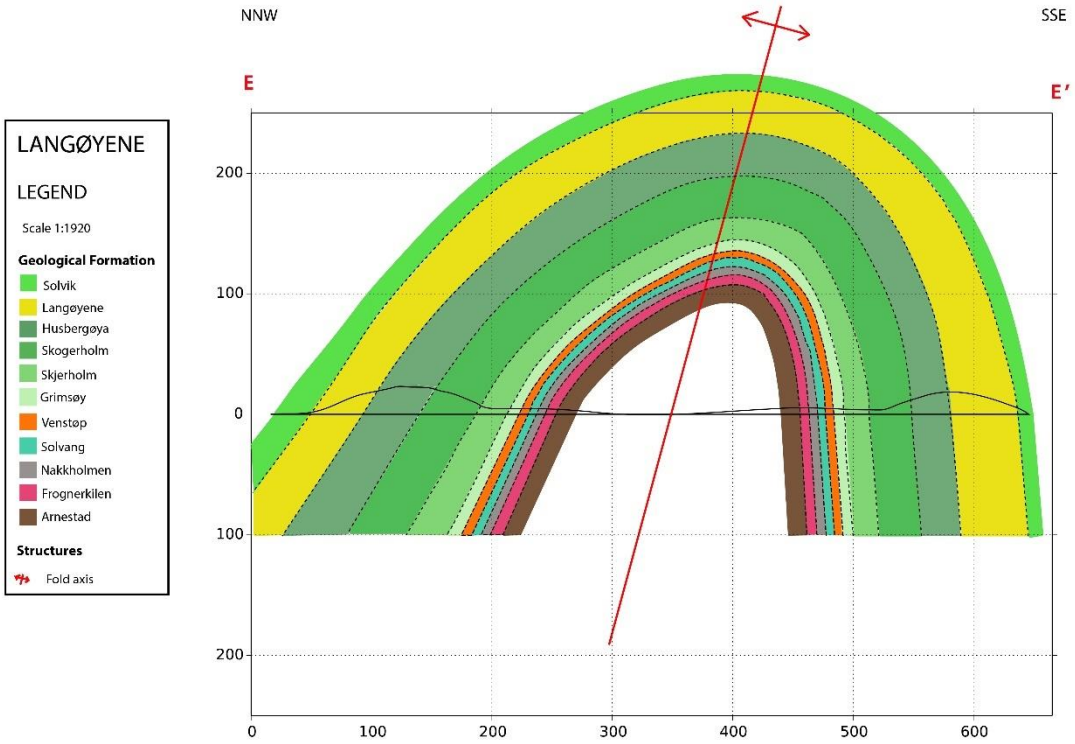

Figure 5.30: Cross section profile of Langøyene (for profile in A3 size, see appendix F)

6 Discussion

Introduction

The results gathered through field work following observations and mapping of geological structures along with data processing will be discussed in this chapter. The field mapping in this thesis and digitalization of new and old results have produced the most detailed map and cross-sections of the Inner Oslofjord between Ekeberg in the east and Nesodden in the west to date (appendix A). The results are used below to discuss some implications for the Oslo Rift.

The mapping confirms that geological structures of Permo-Carboniferous age in the Oslo Region are characterized by numerous, typically NNW and N-striking normal faults and intrusive dikes, which reflect the main stress-axes orientation during the first stages of the Oslo Rift (Freund 1982; Swensson, 1990).

Previous calculations of extension and displacement done on the entire Oslo Rift will be discussed against processed results from the study area. The results will furthermore be discussed on a regional scale within the Oslo Rift, along with two proposed models of rifting:

1) Mantle plume induced rifting

2) Tornquist strike slip fault associated rifting

6.1 Orientation and of extensional faults in the mapping area

The dominant orientation of the Permo-Carboniferous age structures in the study area is NNW-SSE and N-S with a varying dip of 60° to sub vertical. This gives a minimum stress (σ_3) oriented WSW-ENE to EW, and vertical maximum stress (σ_1).

In the study area the Permian extensional structures are located in a fault block within the Oslo Graben, bounded by the Nesodden Fault Segment on the western side and the Ekeberg Fault on the eastern side. A third fault just south of the study area, the Oslofjorden Fault with a N-S to NNE-SSW orientation has given rise to the main trend of the Oslo Graben

(Swensson, 1990). The Ekeberg Fault has an NNW-SSE orientation closely matching the orientation of the main extensional structures in the study area.

The constructed fold axis of the folded islands plunges towards the east, towards the Ekeberg Fault with and average dip of 10°. This shows that the study area fault block rotated towards the Ekeberg Fault. With an estimated dip of ca. 60° the Ekeberg Fault should becogeome more shallow with depth. The major faults separating the islands into smaller fault blocks (appendix A) are not exposed anywhere in the mapped area. Given that the main exposed faults on the islands typically are subvertical, we assume that this is also the case for the hidden faults. However, on Ulvøya, the closest island to the Ekeberg Fault, the constructed fault axis is measured to 0°. This flattening effect towards the rift bounding fault in the east, could be explained by a certain amount of drag against the Ekeberg Fault (fig 6.3c).

6.2 Estimates of extension across the mapping area

Estimates of extension based on thickness of the dikes give a stretching factor of 3%. This is close to what Pallesen (1993) estimated across the Oslofjord Master Fault, south of the study area in an E-W profile from Horten and westwards. The estimates showed a stretching factor of 2-3%, but with locally large variations.

As the study area fault block indicates a certain amount of rotation, calculations on the fault block should be added to the total amount of extension within the Oslo Rift. This was done by a rough estimate based on a 60° dipping fault plane assuming a mean rotation of 9°, based on the calculated plunge of fold axes from each island (fig 6.1 and equation 6.1).

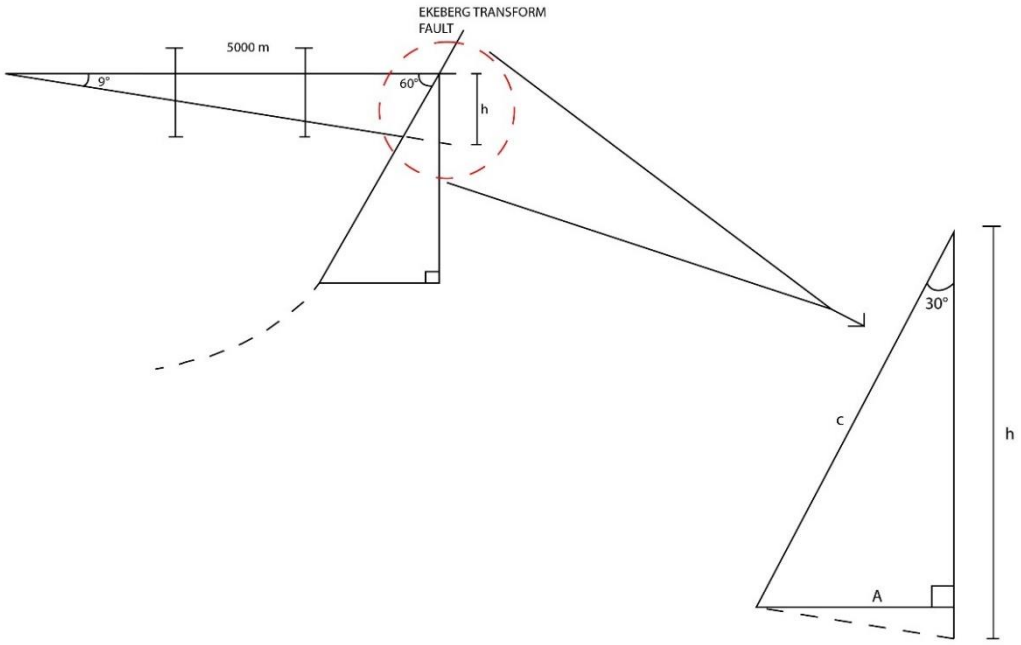

Figure 6.1: Schematic drawing showing how the amount of extension was calculated from the rotated fault block.

$$\tan 10 = \frac{h}{5000}$$

$$h = 881\ m$$

$$\cos 30 = \frac{c}{h}$$

$$c = 763\ m$$

$$\sin 30 = \frac{A}{c}$$

$$A = 381\ m$$

Equation 6.1: Calculation done to estimate amount of extension based on the tilted fault block.

Estimations on the rotated fault blocks suggests a stretching factor of 7%, this would then give a total stretching factor of 10% including both dikes and normal faults within the mapped area. To correlate extension caused by rotated faults against Pallesen (1993) another formula after Wernicke and Burchfiel (1982) must be applied, where φ_i is the original fault plane dip and θ is the dip of the bedding (equation 6.2).

$$\%ext = \left[\left(\frac{\sin(\varphi_i)}{\sin(\varphi_i - \theta}\right) - 1\right] * 100$$

Equation 6.2: Equation after Wernicke and Burchfiel (1982) for rotated planar faults.

This gives a stretching factor of 11.9% just within the minimum and maximum values calculated by Pallesen (1993) of 3-12%. This suggests extension towards the higher degree in the inner Oslofjord. A total stretching factor for the study area based on both dikes and faults would then be 10-15% against Pallesen (1993) 6-20%. In this respect it would seem that the structural extension in the inner Oslofjord reflects those on regional scale. Calculated estimates are presented in table 6.1.

Table 6.1: Comparison with previous and present day work of total stretching factor and vertical displacement on the Oslo Rift. Total amount of vertical displacement calculated here is the combined displacement within the study area + the estimated vertical displacement on the Ekeberg Fault.

THE OSLO RIFT		
BY	***STRETCHING FACTOR***	***TOTAL AMOUNT OF VERTICAL DISPLACEMENT***
This thesis	**10-15%**	**1488 m**
Pallesen (1993)	**6-20%**	**1555-3000 m**
Ro &Faleide (1992)	**13-15%**	**-**

6.3 Origin of the Oslo rift, some observations from field mapping

Extensional faults tend to develop with a dip of 60°, but this does not correspond with what is mapped in the study area. 56% of the recorded minor normal faults within the study area corresponds to the Ekeberg fault of 60°. However, a large proportion of the normal faults in the mapping area have steep dips of approximately (75-90°) and are commonly associated with dikes and large apparent offset. There are four main hypotheses for the generation of steep/subvertical faults in a rift system:

1) Reactivation of pre-existing steep fractures (e.g. joints/strike-slip faults)
2) Low confining pressure (i.e. surface near, little overburden), leading to a dilational stress regime.
3) Rotation of originally shallower dipping faults on a larger listric master fault (in this case the Ekeberg fault)
4) Faulting due to uplift/doming of the lithosphere above a mantle plume.

These four hypotheses are discussed below.

Hypothesis 1:

It has been suggested that the steep faults could be reactivation of pre-existing weak zones, but according to lineaments mapped by Gabrielsen et al. (2018) there are no signs of pre-existing steep structures with a N-S direction outside the Oslo Rift. The lineaments within the study area are more or less perpendicular to what is found outside the Oslo Rift. Based on these observations hypotheses 1) indicating reactivation of pre-existing steep structures can be rejected.

Hypothesis 2:

The closer to the surface, the smaller the confining pressure of surrounding material is. The low pressure close to the surface can result in steeping of faults to subvertical. During the

initial stages of the rift development the exposed section of the study area most likely was located close to the surface. This is based on cross-sections from Naterstad et al. (1990), NGU map, suggesting that 300 m of the surface is missing. This is further supported by the observation that the stratigraphic thickness of the Cambro-Silurian sediments in the Oslo Region is approximately 2 km (Bockelie and Nystuen 1985; Bruton et al. 2010). The presently exposed section in the mapping area in middle Ordovician-lower Silurian. It seems reasonable to interpret the exposed study area to have been within a few km of the surface at the time of rift initiation.

Normal faults of 60° predicted by the Coulomb-Mohr criteria increases with decreasing confined pressure. Under ideal conditions the faults will reach 90° under tension in the absence of confining pressure. This hypothesis could explain the numerous subvertical faults within the study area. This predicts that the dip of the subvertical faults rotate towards 60° with increasing depth.

This hypothesis also implies as rifting continuous and extensive magmatism is extruded above the mapped area (Larsen et al. 2008), new faults developed should become less steep with increasing confining pressure.

No evidence disapproving of this hypothesis is found within the study area.

Hypothesis 3:

Fault planes on the major faults in the area (fig 6.2) have a mean principal orientation of 157/87. These almost subvertical faults could initially have been less step.

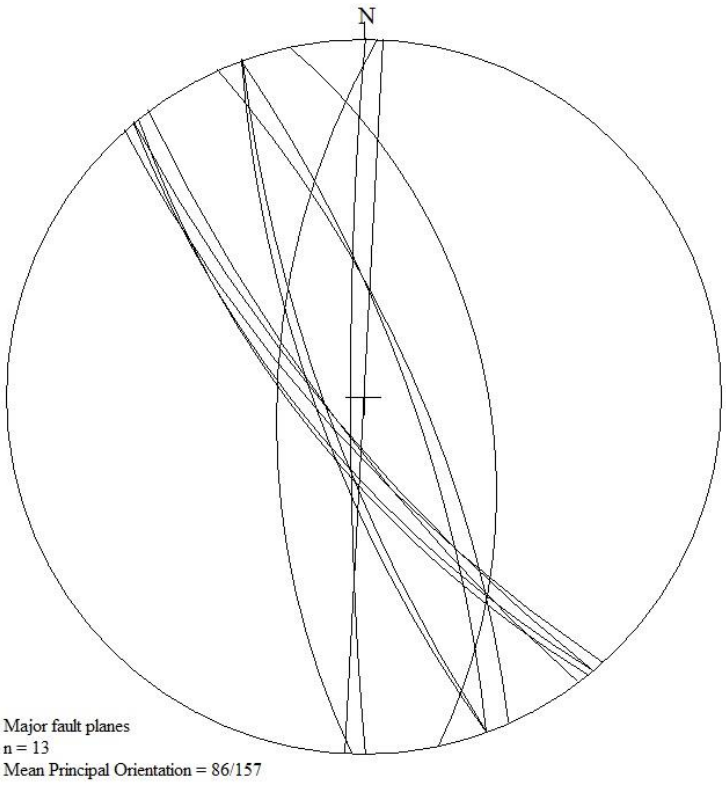

Figure 6.2: Stereographic projection of the major fault planes within the study area.

Pallesen (1993) describes a similar effect further southwest in the Horten area, still within the Oslo Rift. Tilted fault blocks with about 15° rotation to the west are recorded. In this area no fault plane is exposed due to glacial erosion. But 45 km to the north in Slemmestad a well-exposed fault plane with 48° dip is observed. Since there is no way of determining the pre-rotational dips, he suggests that the amount of rotation recorded in Horten could be applied to the fault plane recorded in Slemmestad. This would then give the initial fault plane dip an angle of approximately 60°.

This could also be the case within the study area fault block (fig 6.2). Applying the 15° rotation gives the presently subvertical faults an initial dip of approximately 70° prior to rotation. This does, however, not fit well with the observations from the present study area where the plunge of the fold axes varies from 6° on Hovedøya and Lindøya in the north via 13° on Gressholmen to 14° on Langøyene and 12° on Malmøya further south. This would suggest that there is more rotation of the fault blocks the further south we move. If this is also the case for the faults observed by Pallesen (1993), then the amount of rotation is specific to one segment of a particular fault. Thus, the approach used by Pallesen (1993) would not work.

An alternative explanation could be that Pallesen (1993) followed an E-W transect across the entire Vestfold Graben crossing the Oslofjorden Fault, which is oriented differently from the Ekeberg Fault that affects the present study area. This could again indicate that the different segments of the rift, and by implication the different master faults, have differing geometries.

I propose that the reason for the increasing dip towards south in the study area is because the Ekeberg Fault has an increasing displacement towards the south. This would match the fault pattern south of the Bunnefjord, that suggests that the Ekeberg Fault connects with the Oslofjorden Fault in the south.

A reason for the increasing dip towards the south in the study area could be that the Oslofjorden Fault connects with the Ekeberg Fault in south. This may have caused a scissor effect where the amount of displacement would increase closer to the fault junction.

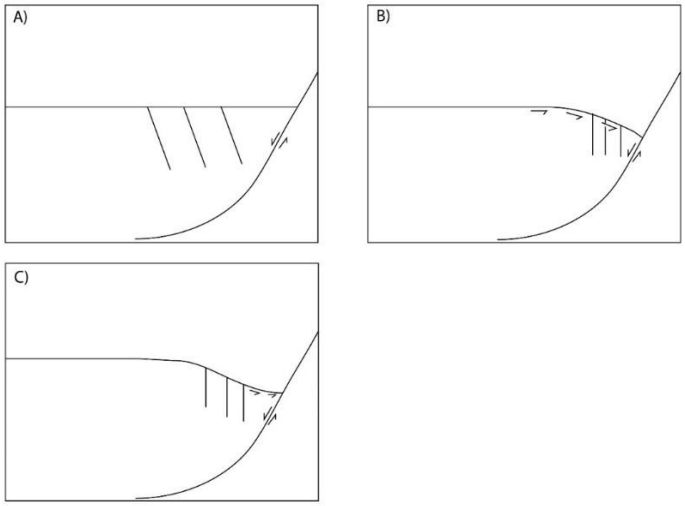

Figure 6.3: Schematic drawing of how the subvertical faults could reflect rotation towards the Ekeberg Fault in a roll-over anticline 6.3A-B. This does not match the observed plunge of the fold axes in the mapped area. In 6.3C the dragfold along the Ekeberg Fault would flatten the rotation against the fault plane. This is proposed as the reason for the horizontal fold axis on Ulvøya.

Hypothesis 4:

One of the hypotheses suggests for the formation of the Oslo Rift suggests that a mantle plume located beneath the Oslo Graben increased the temperatures in the asthenosphere (Torsvik et al. 2008). This process resulted in dynamic uplift of the lithosphere (fig 6.4). This is active rifting initially associated with little extension, steep radial faults and extensive magmatism (Gabrielsen, 1986; Fossen, 2010). The calculations performed on dikes and tilted normal faults indicate little extension within the study area. The field observations suggest

that the fault blocks in the field area have subsided along these subvertical faults, with little additional formation of normal extensional faults at 60°. The amount and prevalence of dikes in the field area, and the large intrusives and extrusives in other parts of the Oslo Rift (Larsen et al. 2008) indicate extensive magmatism during rifting. Thus, the available field observations are compatible with an active rift associated with a mantle plume.

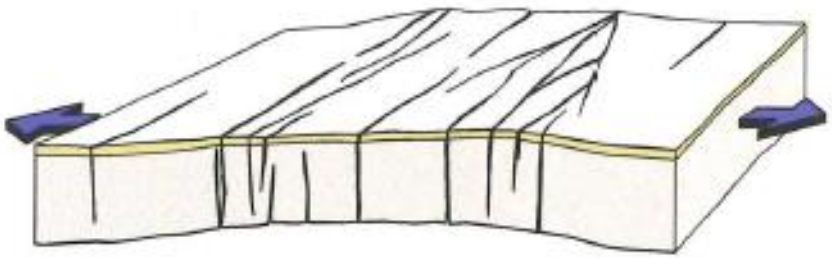

Figure 6.4: Initiation of an active rift is accosiated with the formation of radial (steep) faults and fractures. From Fossen (2010).

As an alternative, it has been proposed that the Oslo Rift started as a passive rift associated with dextral movements along the Tornquist zone, and over time developed into an active rift (Heeremans et al. 1996). This has been an ongoing debate. One possible criterion to separate these two models could be the presence of initial doming and formation of subvertical radial faults in an active rift, and its absence in a passive rift. However, due to the close proximity of the field area to the surface at the time of initial rifting, the steep faults in the inner Oslofjord could also reflect this near surface stressfield. Hence, the present data set cannot differentiate between the two models. However, the active rift model predicts that the subvertical faults continue downwards, whereas the passive model predicts that they shallow to 60° with increasing depth. This could in the future be tested with seismic data.

7 Conclusion

From the measurements recorded in the mapped area and data processing it is evident that there has been little extension in the Oslo Graben, with only a stretching factor of 10-15% based on calculated displacement and intrusive dikes. The subvertical normal faults and extensive magmatism in the form of dikes could suggest that the triggering factor of the Oslo Rift was active rifting, but passive rifting cannot be ruled out.

It is hard to differentiate the two modes based on the exposed surfaces in the mapped area, so future work with seismics from the same area could help in concluding the real cause of the Oslo Rift.

References

Andersen, T.B. 1998. Extensional tectonics in the Caledonides of southern Norway, an overview. *Tectonophysics* 285, 333-351.

Baarli, B. G. 1985. The stratigraphy and sedimentology of the early Llandovery Solvik Formation in the central Oslo Region, Norway. *Norsk geologisk tidsskrift* 65 (4), 255-275.

Bjørlykke, K. 1974. Geochemical and mineralogical influence of Ordovician Island Arcs on epicontinental clastic sedimentation. A study of Lower Palaeozoic sedimentation in the Oslo Region, Norway. *Sedimentology* 21, 251-272.

Bocklie, J.F and Nystuen, J.P. 1985. The southeastern part of the Scandinavian Caledonides. *In*: Gee, D.G and Sturt, B.A. (eds.), *The Caledonide Orogen – Scandinavia and Related areas*. John Wiley & Sons, Chichester, 69-88.

Brenchly, D.J and Newall. G. 1980. A facies analysis of Upper Ordovician regressive sequences in the Oslo Region. Norway – a record of glacio-eustatic changes. *Palaeogeography, Palaeoclimatology, Palaeoecology* 31, 1-38.

Bruton, D.L., Gabrielsen, R.H. and Larsen, B.T. 2010. The Caledonides of the Oslo Region, Norway – stratigraphy and structural elements. *Norwegian Journal of Geology* 90, 93-121.

Brøgger, W.C. 1885. Geologisk kart over öerne ved Kristiania (Etagen 4). På grundlag af kart over Kristiania havnedistrikt opptaget 1884 og 1885. Målestokk 1:10.000; 1885; General-stabens Litografiske Anstalt, Stockholm; Sidetall 1 kart.

Cocks, L.R.M. and Torsvik, T.H. 2005. Baltica form the late Precambrian to mid-Palaeozoic times: The gain and loss of a terranes identity. *Earth-Science Reviews* 72, 39-66.

Corfu, F. and Dahlgren, S. 2007. Perovskite U-Pb ages and Pb isotopic composition of alkine volcanism initiating the Permo-Carboniferous Oslo Rift. *Earth and Planetary Science Letters* 265, 256-269

Dehli, G. 2012. *The geometry and structural development of Caledonian folds and faults, inner Oslofjord*. Master thesis in geosciences. University of Oslo. 124 pp.

Dutrow, B. and Klein, C. Mineral Assemblages: Introduction to Rock Types. *In:*Dutrow, B., Klein, C. *THE 23 RD EDITION of THE MANUAL OF MINERAL SCIENCE*. Johan Wiley & Sons. 574-603.

Fossen, H. 2010a. Folds and folding. *In*: Fossen, H. *Structural Geology*. Cambridge University Press. 219-241.

Fossen, H. 2010b. Extensional regimes. *In*: Fossen, H. *Structural Geology*. Cambridge University Press. 333-353.

Fossen, H, Pedersen, R.B, Bergh, S and Andresen A. 2008. Creation of a mountain chain. THE Building Up Of The Caledonides: About 500-405 million years. *In*: Ramberg, I.B, Bryhni, I, Nøttvedt, A, Rangnes, K. (eds.) 2008, *The Making of a Land – Geology of Norway*. Trondheim. Norsk Geologisk Forening, 181-231.

Freund, R. 1982. The role of shearing in rifting. *In*: Pàlmason, G (Editor). 1982, *Continental and Oceanic Rifts*. American Geophysical Union, Geodynamics 8, 33-40.

Gabrielsen, R.H., Nystuen, J.P., Olesen, O. 2018. Fault distribution in the Precambrian basement of South Norway. *Journal of Structural Geology* 108, 269-289.

Gee, D.G. 1975. A tectonic model for the central part of the Scandinavian Caledonides. *American Jounral of Science* 275 (A), 468-515

Gee, D.G., Fossen, H., Henriksen, N. and Higgins, A.K. 2008. From the Early Paleozoic Platforms of Baltica and Laurentia to the Caledonide Orogen of Scandinavia and Greenland. *Episodes* 31 (1), 44-51.

GEONORGE:

Kartverket. 2015/19.04.2018. *Dybdedata WMS*. Available at: https://openwms.statkart.no/skwms1/wms.dybdedata?request=GetCapabilities&service=WMS (22.05.2018).

Groshong, R.H.2006. Cross section, Data Projection and Dip-Domain Mapping. In Groshong, R.H. (ed.) 3-D Structural Geology: *A practical Guide to Quantitative surface and subsurface Map Interpretation*. 2nd ed. Berlin: Springer, 133-180.

Harper, D.A.T. and Owen, A.W. 1983. The structure of the Ordovician rocks of the Ringerike district: evidence of a thrust system within the Oslo Region. *Norsk Geologisk Tidsskrift* 63, 111-115.

Heeremans, M., Lasen, B.T. and Stel, H. 1997. Paleostress reconstruction from kinematic indicators in the Oslo Graben, southern Norway: new constraints on the mode of rifting. *Tectonophysics* 266, 55-79.

Holcombe, R. 2011. *GeoOrient*. Available at: http://www.holcombe.net.au/software/ (Accessed: 05.03.2018).

Hossack, J.R and Copper, M.A. 1986. Collison tectonics in the Scandinavian Caledonides. *Geological Society, London, Special Publications* 19, 285-304.

Hurich, C.A., Dyrelius, H.P.D. and Kristoffersen, Y. 1989. Deformation of the Baltic continental crust during Caledonide intracontinental subduction: Views from seismic reflection data. *Geology* 17, 423-425.

Korja, T., Smirnov, M., Pedersen, L.B. and Gharibi, M. 2008. Structure of the Central Scandinavian Caledonides and the underlying Precambrian basement, new constraints from magnetotellurics. *Geophysical Journal International* 175, 55-69.

Larsen, B.T. and Olaussen, S. 2005. The Oslo Region. A study in classical Palaeozic Geology. Field guide to NGFs Centennial Field Trip 26-28. May 2005. *Norsk Geologisk Forening*, 88pp.

Larsen, B.T., Olaussen, S., Sundvoll, B. and Heeremans, M. 2008b. The Permo-Carboniferous Oslo Rift through six stages and 65 million years. *Episodes* 31 (1). 52-58.

Larsen, B.T., Olaussen, S., Sundvoll, B. and Heeremans, M. 2008a. Volcanoes and faulting in arid climate. The Oslo Rift and North Sea in the Carboniferous and Permian, 359-251 Million Years Ago. *In*: Ramberg, I.B, Bryhni, I, Nøttvedt, A, Rangnes, K. (eds.) 2008, *The Making of a Land –Geology of Norway*. Trondheim. Norsk Geologisk Forening, 181-231.

McCann, T., Pascal, C., Timmerman, M.J., Krzywiec, P., Lòpez-Gòmez, J., Wetzel, A., Krawczyk, C.M., Rieke, H. and LaMarche, J. 2006. Post-Variscan (end Carboniferous-Early Permian) basin evolution in Western and Central Europe. *In*: Gee, D.G., and Stephensson, R.A. (eds.) *European Lithosphere Dynamics*. Geological Society of London, Memoirs 32, 355-388.

Morley, C.K. 1986a. The Caledonian thrust front and palinspastic r-estorations in the southern Norwegian Caledonides. *Journal of Structural Geology* 8 (7), 753-765.

Morley, C.K. 1986b. Vertical strain variations in the Osen-Røa thrust sheet, North-western Oslo Fjord, Norway. *Journal of Structural Geology* 8 (6), 621-632.

Morley, C.K. 1987. Lateral and vertical changes of deformation style in the Osen-Røa thrust sheet, Oslo Region. *Journal of Structural Geology* 9 (3), 331-343.

Morley, C.K. 1994. Fold-generated imbricates: examples from the Caledonides of Southern Norway. *Journal of Structural Geology* 16 (5), 619-631.

Nakrem, H.A. and Worsley, D. 2008.The Lower Palaeozic. Cambrium, Ordovician and Silurian – The Sea Teems With Life 542-416 Million Years. *In*: Ramberg, I.B, Bryhni, I, Nøttvedt, A, Rangnes, K. (eds.) 2008, *The Making of a Land –Geology of Norway*. Trondheim. Norsk Geologisk Forening, 181-231.

Natterstad, J., Bockelie, J.F., Bockelie, T., Graversen, O., Hjelmeland, H., Larsen, B.T., Nilsen, O. 1990. Asker 1814 I, berggrunnskart M. 1:50000. *Norges geologiske undersøkelse*.

Neumann, E.R., Olsen, K.H., Baldrigde, W.S. and Sudnvoll, B. 1992. The Oslo Rift: a review. *Tectonophysics* 208, 1-18.

Nystuen, J.P. 1981. The late Precambrian "Sparagmites" of Southern Norway: A major Caledonian Allochthon – The Osen-Røa Nappe Complex. *American Journal of Science* 281, 69-94.

Owen, A. W., Bruton, D.L., Bockelie, F.J. and Bockelie, T.G. 1990. The Ordovician succession of the Oslo Region, Norway. *Norges geologiske undersøkelse,* Special publication 4, 55 pp.

Pallesen, S. 1993. Crustal extension in the Oslo Graben, SE Norway: a method incorporating magmatism and erosion. *Tectonophysics* 221, 155-172.

Ramberg, I.B., Gabrielsen. R.H., Larsen, B.T. and Solli, A. 1977. Analysis of fracture pattern in southern Norway. *Geologie en Mijnbouw* 56, 295-310.

Ramberg, I.B. and Spjeldnæs, N. 1978. The Tectonic History of the Oslo Region. *In*: Ramberg, I.B., Neumann, E.R. (eds.) *Tectonics and Geophysics of Continental Rifts*. NATO ASI Series. Series C 37. Dordrecht: Reidel, 167-194.

Ramsay, J.G. 1967. *Folding and Fracturing of Rocks*. New York, Wiley, 568 pp.

Repshus, J.G. 2012. *Caledonian structural development on Hovedøya and Lindøya, in the inner Oslofjord*. Master thesis in geosciences. University of Oslo. 98 pp.

Ro, H.E. and Faleide, J.I. 1992. A stretching model for the Oslo Rift. *In*: P.A Ziegler. *Geodynamics of Rifting Volume 1. Case History Studies on Rifts: Europe and Asia*. Tectonophysics 208, 19.36.

Roberts, D. 2003. The Scandinavian Caledonides: event chronology, palaeographic settings and likely modern analogues. *Tectonophysics* 365, 283-299.

Roberts, D and Gee, D.G. 1985. An introduction to the structure of the Scandinavian Caledonides. *In*: Gee, D.G., and Sturt, B.A. (eds). The Caledonide Orogen-Scandinavia and Related Areas. *Wiley*, 55-68.

Sundvoll, B., Neumann, E.R., Larsen, B.T. and Tuen, E. 1990. Age relations among Oslo Rift magmatic rocks: implications for tectonic and magmatic modelling. *Tectonophysics* 178, 67-87.

Swensson, E. 1990. Cataclastic rocks along the Nesodden Fault, Oslo Region, Norway: a reactivated Precambrian shear zone. *Tectonophysics* 178, 51-65.

Torsvik, T.H., Smethurst, M.A., Burke, K, Steinberger, B. 2008. Long term stability in deep mantle structure: Evidence from the -300 Ma Skagerrak-Centered Large Igneous Province (the SCLIP). *Earth and Planetary Science Letters* 267, 444-452.

Wernicke, B and Burchfiel, B.C. 1982. Modes of extensional tectonics. *Journal of Structural Geology* 4, 105-115.

Worsley, D., Aarhus, N., Basset.G.M., Howe, M.P.A., Mørk, A.M. and Olaussen, S. 1983. The Silurian succession of the Oslo Region. *Norges geologiske undersøkelse* 384, 1-57.

Ziegler, P.A., Schumacher, M.E., Dèzes, P., Van Wees, J.D. and Cloething, S. 2006. Post Variscan evolution of the lithospehere in the area of the European Cenozoic Rift System. *In*: Gee, D.G., and Stephensson R.A. (eds.) *European Lithosphere Dynamics*. Geological Society of London, Memoirs 32, 97-112.